Role of GCN5 and PCAF during B Lymphocyte Development

Thesis for master degree

KHAC THANH PHONG CHAU

Department of Biotechnology and Food Science

Faculty of Natural Sciences

Norwegian University of Science and Technology, Trondheim

07.2018

Supervisors: Valentyn Oksenych, PhD (Faculty of Medicine and Health Sciences)

Carole Beck, PhD (Faculty of Medicine and Health Sciences)

Internal supervisor: Finn Lillelund Aachmann, PhD (Faculty of Natural Science)

ABSTRACT

Millions of B lymphocytes are generated every day to protect the host against pathogens. To complete the journey from bone marrow as hematopoietic stem cells to periphery as mature B cells, lymphocytes need to undergo carefully regulated sequence of events such as V(D)J recombination and class switch recombination (CSR) that mainly depend on double-strand breaks (DSBs). When DSBs are induced, dozens of DNA damage response (DDR) factors are recruited at the damaged sites. To facilitate this recruitment, histone acetyltransferases (HATs) such as GCN5 and PCAF participate to reduce the interaction between histones and DNA. Previous studies showed that $Gcn5^{-/-}Pcaf^{-/-}$ mice and $Gcn5^{-/-}$ mice died embryonically while $Pcaf^{-/-}$ mice had no obvious phenotype. Due to the role in DNA damage response and transcription, GCN5 and PCAF could be involved in development of B lymphocyte although it remained unappreciated. To reveal this mystery, I deleted these HATs genes in human HAP1, and in murine vAbl and CH12F3 cell lines by applying CRISPR/Cas9-editing strategy. Subsequently, functional analyses such as proliferation assay and cell cycle analysis were performed in HAP1 cell lines; V(D)J recombination and CSR together with proliferation assay were performed in vAbl and CH12F3 cell lines, respectively. I found that GCN5 is involved in multiple stages of B cell development while PCAF seemed to be dispensable. In addition, GCN5 and PCAF may have the overlapping functions.

ACKNOWLEDGEMENT

Contents

LIST OF FIGURES

LIST OF TABLES

KEY TO ABBREVIATIONS

53BP1   p53 binding protein 1

ATM   ataxia talengiectasia mutated

ATR   ataxia talengiectasia and Rad 3 related

BRCA   breast cancer susceptibility protein

BSA   Bovine Serum Albumin

CSR   class switch recombination

DDR   DNA damage response

DKO   double knockout

DNA   deoxyribonucleic acid

DNA-PK.   DNA dependent protein kinase

DNA-PKcs   DNA dependent protein kinase catalytic subunit

DSB   double strand break

G1 phase   gap 1 phase

GCN5   General control of amino acid synthesis protein 5

H2AX   histone 2A variant X

HR   homologous recombination

MDC1   mediator of DNA damage checkpoint protein 1

MRN   MRE11, RAD50, NBS1

NHEJ   non-homologous end-joining

PAGE   polyacrylamide gel electrophoresis

PAXX   paralog of XRCC4 and XLF

PCAF   p300/CBP-associated factor

RAG   recombination activation gene

RSS   recombination signal sequence

SSB   single strand break

TdT   terminal de-oxy transferase

V(D)J	variable, diversity, joining
WT	wild-type
XLF	XRCC4 like factor
XRCC4	X-ray cross complementing protein 4

1. Introduction

When James Watson and Francis Crick presented the molecular structure of DNA in 1953 (Watson J and F Crick, 1953), it was believed to be stable for maintaining the genetic information and crucial for the development as well as functioning of an organism. However, later studies showed that DNA was vulnerable for damages that could arise from environment conditions or by various mechanisms occurring inside the cells.

The damages in DNA have both positive and negative side effects depending on where the mutation locates and which kind of cell mutation arises at. During evolution, DNA damage contributes to the genetic diversity and selection in the nature; in the cellular aspect, the DNA damage leads to the mutation and cell death. In contrast to different biomolecules, DNA cannot be replaced, but it can be repaired only.

To combat the threats coming from both the endogenous and environmental DNA damages, eukaryotic cells have developed a system of DNA lesion sensors to detect this event and activate the DNA damage response (DDR) at which the chromatin-related modifications are at the heart (Carrassa L and Damia G, 2017). Sensing of DNA lesions activates the cell cycle checkpoint and cell cycle arrest to give adequate time for DNA repair. To encounter different kinds of lesions, a network of repair mechanisms has been evolved. DNA repair pathways such as Base Excision Repair (BER), Mismatch Repair (MMR), Homologous Recombination (HR) and Non-Homologous End Joining (NHEJ) are found in all organisms and many enzymes are highly conserved from bacteria to human. Different types of DNA damages and DNA repair mechanisms to repair these damages are introduced in the next parts. Defects in DDR and DNA repair can lead to carcinogenesis and degenerative diseases (Saez, 2017).

1.1. DNA damage

DNA damage can be caused by exogenous factors including environment factors or endogenous factors or cellular metabolic processes (Tubbs and Nussenzweig, 2017). Furthermore, the chemical instability of DNA also leads to the spontaneous damage occurring at a high rate.

Genotoxic chemicals, thermal disruption, radiation and viruses are the main environment contributors. Typically, industrial chemical can cause a diversity of DNA adducts such as

oxidation and alkylation. Thermal disruption can cause the DNA single strand breaks at the elevated temperature. Viruses may cause the damage to the host chromosome by integrating of viral DNA. The major exogenous DNA damaging agents are ionizing radiation (IR) and ultraviolet (UV) radiation. Ionizing radiation generates both reactive oxygen species (ROS) and reactive nitrogen species (Tubb and Nussenzweig, 2017). Although UV light has the lower energy compared to that of ionizing radiation, it is a potent mutagen for organism. Two major products of UV absorption by pyrimidines are pyrimidine hydrates and pyrimidine dimers, including cyclopyrimidine dimers, 6,4-photoproducts and dewar dimers. These DNA lesions are led by perturbing the DNA double helices, interfering with the accurate DNA replication and inducing UV thymine dimers (Tubb and Nussenzweig, 2017).

Cellular metabolism processes also cause DNA damage. Precise and accurate DNA replication is the important event that occurs during S phase in cell cycle to produce two identical DNA replicas from the original one. During this, some DNA polymerases may replicate DNA with low fidelity. Moreover, meiosis is also a source of DNA damage. During meiosis, parental and maternal homologous chromosomes pair and align together along their length to exchange the genetic material. To achieve this exchange, double strand breaks (DSBs) are introduced (Lukaszewicza *et al*, 2017). In addition, during the development of B lymphocytes, cells undergo two DSBs-dependent mechanisms: V(D)J recombination and class switch recombination (CSR) (Nicolas L *el al,* 2018). My project was focusing on these mechanisms.

1.2. DNA repair pathways

To encounter challenges caused by DNA damage, several DNA repair pathways have been evolved. There are more than 130 DNA repair genes that have been identified in human so far. These genes are involved in repairing of DNA lesions. DSBs are repaired either by homologous recombination (HR) or the non-homologous end joining (NHEJ) (Jeggo and Lobrich, 2017). Excision repair is carried out by nucleotide excision repair (NER) and base excision repair (BER). NER removes bulky DNA lesions (Saez, 2017) and base excision repair (BER) corrects DNA damage from oxidation, deamination and alkylation of nucleotides (Carter and Parsons, 2016). Mismatch repair (MMR) removes errors appeared during the DNA replication (Hsieh and Zhang, 2017) (Figure 1.1). In addition, it has been reported that these pathways efficiently repair the DNA damages caused by various damage-induced factors such as irradiation or chemicals (Saez, 2017).

The multiplicity of repair pathways that have evolved in organisms ranging from bacteria to humans suggests the importance of keeping mutation and DNA lesions at a tolerable level. Or else, DNA mutations will cause severe damages to human health including cancer, rapid ageing and shortened life span as well as various other syndromes.

1.2.1. Single-strand breaks (SSBs) repair mechanisms

Mismatch repair (MMR) removes the deletions and insertions in DNA caused by DNA replication slippage and mismatches caused by DNA polymerases errors during DNA replication (Hsieh and Zhang, 2017). Base excision repair (BER) removes the DNA with small chemical modifications by excision damaged bases from backbone. In addition, BER can repair the apurinic/apyrimidine sites and single-strand breaks (Carter and Parsons, 2016). Nucleotide excision repair (NER) repairs different DNA lesions, including bulky DNA lesions such as pyrimidine dimers. NER can be divided into two sub pathways global genome NER (GGR) and transcriptional-coupled NER (TCR). GGR is used to detect and remove the lesions through the genome while TCR repairs genes that are actively transcribed (Saez, 2017).

1.2.2. Double-strand break repair mechanisms

Homologous recombination (HR) and non-homologous end joining (NHEJ) are main pathways to repair DSBs (Jeggo and Lobrich, 2017). In HR, the strand exchange between DNA occurs while in NHEJ, there is a direct joining of free DNA ends and thus, NHEJ is believed to be faster than HR. In addition, the cell cycle phases also are important for the choice between two pathways. NHEJ is activated through all cycle while in S/G2 phases, HR is the main mechanism when sister chromatids are available as templates for repair (Lobrich and Jeggo, 2017). In this project, I focused on the NHEJ repair mechanism, which is described in detail below.
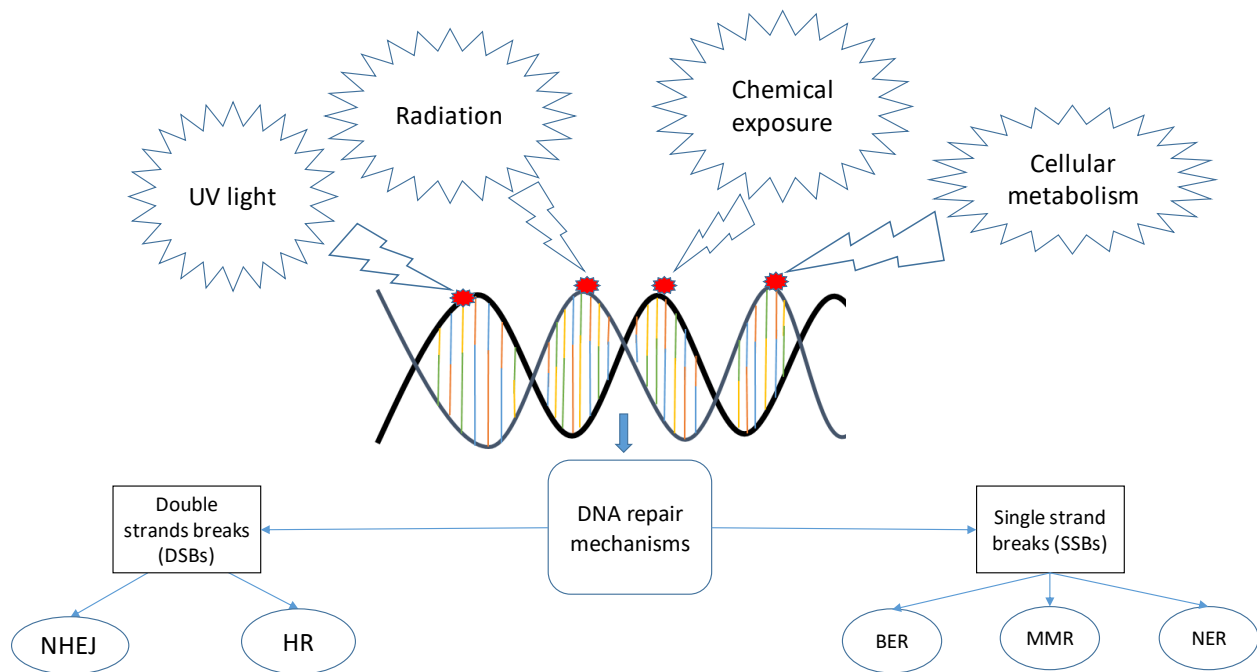
Figure 1.1. Overview of DNA repair pathways. DNA can be damaged by both endogenous and exogenous factors. To resolve DNA lesions, different pathways of DNA repair have been developed. SSBs can be repaired by BER, MMR or NER while NHEJ and HR are the main pathways to restore DSBs.

1.2.3. Non-homologous end joining (NHEJ)

There are two types of NHEJ: Classical NHEJ (C-NHEJ) and alternative-end joining (A-EJ) (Chakraboty *et al,* 2016). C-NHEJ is used, for example, to repair the damages arising during B cell development, particularly during V(D)J recombination and class switch recombination (Verkaik *et al,* 2002; Cortizas *et al,* 2013) (Figure 1.2). The first steps in C-NHEJ are recognition and binding to the damaged sites of DNA. This pathway is quickly initiated by the Ku heterodimer composed of Ku70/80 (Ku). Ku binding to DNA ends is only efficient as a heterodimer. In evolution, Ku70 and Ku80 were evolved from the same single ancestor genes and both proteins today contain the C-terminal nuclear localization sequences that allow DNA binding. In addition, around 20bp damaged DNA can bind to this heterodimer because of Ku ring-like structure. Ku heterodimer showed the higher affinity for the DSBs and much weaker for SSBs. Upon binding to DSBs, Ku heterodimer helps to protect DNA ends from nucleolytic degradation (Liu *et al,* 2017).
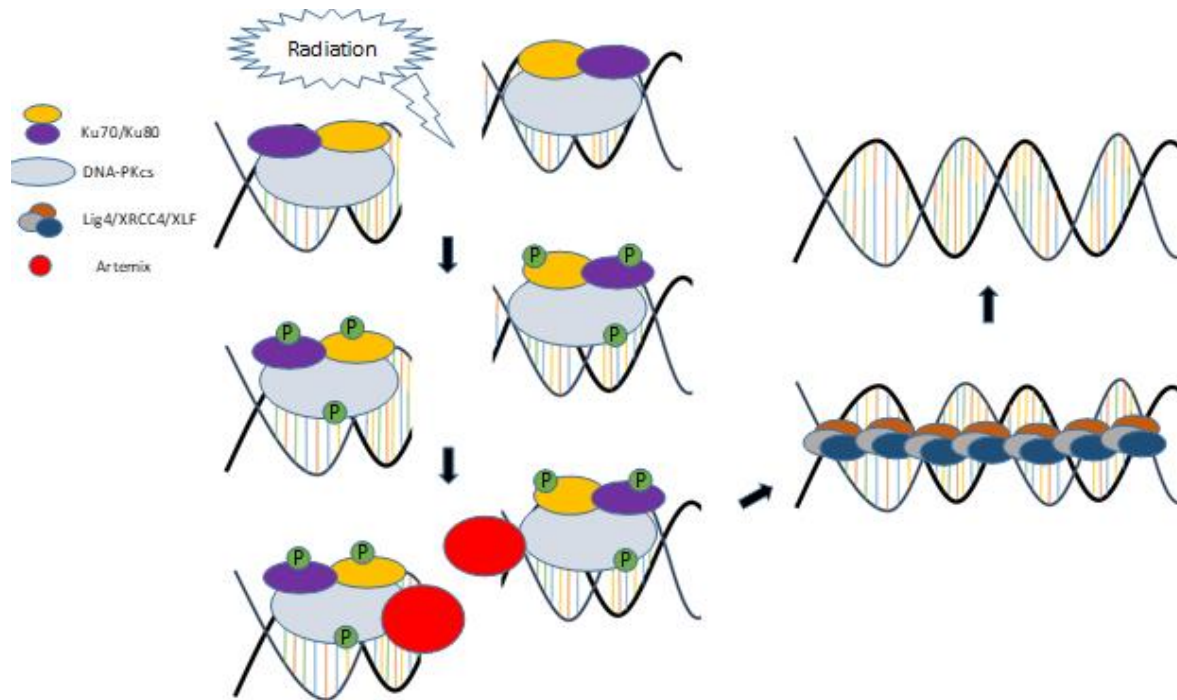
Figure 1.2. DSB repair by NHEJ. This pathway recognizes and rejoins broken DNA ends, often requires trimming of DNA before ligation can occur. In NHEJ, broken DNA ends are bound by Ku70/80 heterodimers, which then recruits the DNA-PKcs. Protein kinase DNA-PKcs phosphorylates and activates additional repair proteins including Artemis. Subsequently, Artemis processes DNA ends prior to ligation. The DNA ends are rejoined by ligase complex including XRCC4, XLF and Lig4.

In addition, when the Ku70/80 heterodimer binds to the DNA ends, it acts as a scaffold protein to recruit other NHEJ core and accessory factors to the damaged sites. First, DNA-PKcs is recruited to form together with Ku holoenzyme, DNA-PK. DNA-PKcs is a protein approximately 4100aa (Bancinyane *et al,* 2017). Structurally, the C-terminus of DNA-PKcs falls into the PI3K kinase family (Dong *et al,* 2018); C-terminal domains are responsible for the kinase activity and N-terminus contains the repeats required for protein-protein interaction. Upon binding to Ku heterodimer, DNA-PKcs kinase activity is increased dramatically. This activity is important to phosphorylate all NHEJ factors itself such as Artemis and defects in DNA-PKcs result modest to severe DNA repair defects, depending on species and mutation (Kumar, Alt, Oksenych, 2014; Bancinyane L et al, 2017).

X-ray cross complementing protein 4 (XRCC4) is another core NHEJ factor recruited to the DSBs by Ku heterodimer. XRCC4 does not have any enzymatic activity and in term of structure, it

contains three parts: globular head domain, alpha-helical stalk and a C-terminal tail. XRCC4 interacts with Ku heterodimer via Ku70 subunit. XRCC4 is also connected to XRCC4-like factor, XLF. DNA Ligase IV (Lig4) is the enzyme interacting with XRCC4. Lig4 contains C-terminal BRCT domain and linker regions that connect two regions together. The first BRCT domain facilitates Lig4 binding to Ku heterodimer while the second one facilitates the interaction between Lig4 and alpha-helical stalk of XRCC4 (Chang *et al,* 2016). Recently, human PAXX, paralog of XRCC4 and XLF was identified and shown to interact with Ku to stabilize NHEJ (Ochi *et al,* 2015, Xing *et al,* 2015, Craxton *et al*, 2015).

After formation of NHEJ complex at the DSBs, its factors start to exert their functions. First, XRCC4-XLF facilitates the formation of filament structure (Hammel *et al,* 2010; Wang *et al*, 2018). This is in complex with Ku heterodimer and DNA-PKcs to generate the DNA ends protection complex (Davis and Chen, 2013; Wang *et al*, 2018). Then, the DNA is processed to generate the ligatable ends. Artemis is responsible for processing due to its endonuclease activity. Artemis cannot fulfill its duty without being phosphorylated by DNA-PKcs or ATM (Jiang, Shan Zha *et al,* 2015; Chang *et al,* 2016). After being processed and before being ligated, filling gaps in DNA are performed by DNA polymerases μ and λ. The final step in the DNA repair pathway is ligation of the broken ends performed by DNA Lig4. This enzyme ligates compatible ends and this activity is also stimulated (Gu *J et al,* 2007) by other factors in the NHEJ complex (Grawunder *et al,* 1997). Once DSBs are repaired, NHEJ complex needs to be removed.

1.3. B cell development
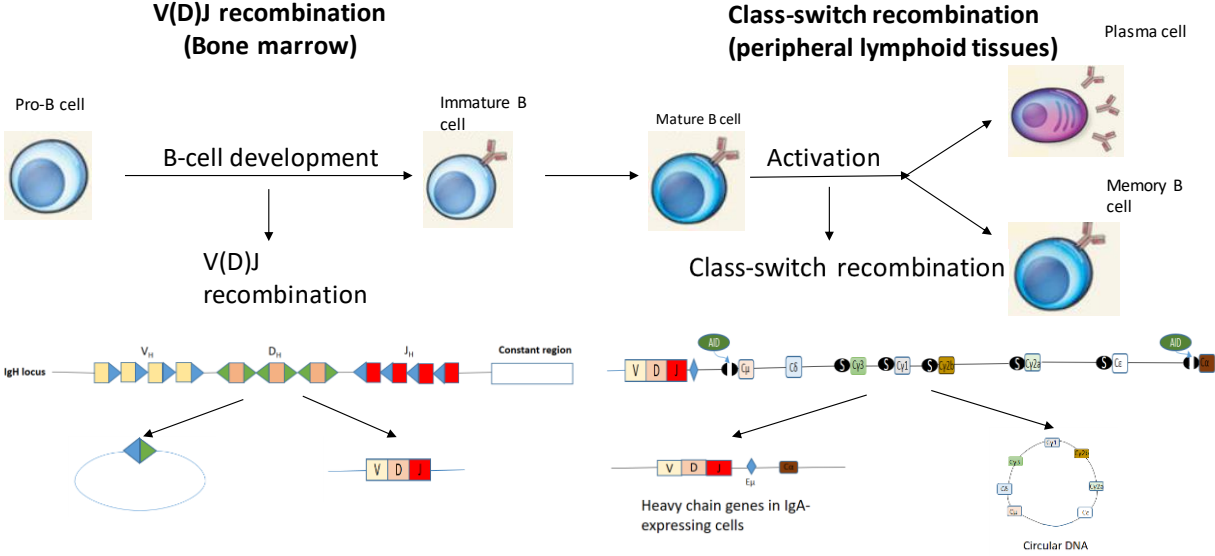
Figure 1.3. The B cell development phases. B cells are created in the bone marrow from pluripotent haemopoietic cells by rearrangement of immunology heavy-chain and light-chain genes. Pro-B cells undergo V(D)J recombination and become pre-B cells expressing IgL with the surrogate light chains. After this phase, immature B cells pair light chains with the μ chains to form the monomeric IgM. The newly synthesized immature B cells exit the bone marrow to enter the peripheral lymphoid tissues . In this environment, they continue to undergo the somatic hypermutation and CSR.

In nature, the diversity of microorganism poses the constant threats to the survival of higher order animals due to their properties, including short reproductive cycle which endows the potential pathogens with the ability to mutate and evolve mechanism to evade host clearance. To erase the dangerous potential arising from these microorganisms, the evolution of mammals resulted in the development of both innate and adaptive immune systems to ensure host survival and reproduction.

B lymphocytes are responsible for the antibody production and T lymphocytes for cell-mediated immune response. B lymphocyte development is the focus of this report.

B lymphocytes express the cell surface immunoglobulin (Ig) receptors that can recognize antigens (Hoffman *et al,* 2016). These immunoglobulin molecules are expressed on the cell surface and secreted to the extracellular space, called antibodies, to neutralize the microbes.

As Figure 1.3 shows, B-cell development is initiated in bone marrow by the dedication of haematopoietic stem cells to the B- cell lineage and is completed with the generation of mature – B cells in peripheral secondary lymphoid organs (the spleen). During first stage of the development, cells are called pro-B and are characterized by the rearrangement of the Ig heavy chain. Different gene segments encode the light- and heavy- chain genes of antibody by rearranging during a process called V(D)J recombination. Specifically, heavy chains are made up of three gene segments: *Variable (V)*, *Diversity (D)* and *Joining (J)* whereas light chain only consists of *V* and *J* segments (Hoffman *et al,* 2016). In general, these combinatorial rearrangements, together with deletions and insertions occurred during V(D)J recombination and supported by TdT and DNA polymerases, allows for large diversity of antibodies to be produced (Murphy and Weaver, 2017). This rearrangement of *Ig* gene segments in B cells is unique and it helps to distinguish B cells from all other blood cells. If V(D)J recombination is not accomplished at this stage, pro-B cells undergo the apoptosis and are eliminated for further development (Murphy and Weaver, 2017). In this stage, the *Ig* α and *Ig* β are expressed at the cell surface together with the calnexin. Upon the successful recombination of heavy chain, pre-B cell receptor (pre-BCR) is formed via the combination of Ig α, Ig β and surrogate light chain (Hoffman *et al,* 2016). At this stage, the light chain V and J fragments are recombined and the successful formation of BCR marking the transition to the immature stage (Hoffman *et al,* 2016).

The newly generated immature B cells enter the environment containing the autoantigens. B cells that express low-affinity autoreactive BCRs are eliminated out of bone marrow and join into the peripheral pools. More than 85% of the newly formed immature B cells die in bone marrow implicating the negative effect of autoantigen recognitions (Nemazee, 2017).

The development from immature to mature B cells are the main event in the spleen and only B cells that are presented in the peripheral pools can be used due to their abilities of recognizing the foreign antigens. B cells are propagated in the antigen-presenting microenvironment at which they undergo several modifications, such as somatic hyper mutation (SHM) and CSR to induce a better fit to the foreign antigens (Bahjat and Guikema, 2017). Typically, SHM introduces the point mutation in the assembled V regions in the DNA of mature B cells. CSR removes the exons in the *IgM* constant region, bringing the functional *VDJ* gene segment closer to the exons of downstream *Ig* constant (*IgC*) regions. The latter process allows the switching from genes encoding low-affinity

antibody IgM to genes that encode high-affinity antibodies, IgG, IgA or IgE isotypes (Bahjat and Guikema, 2017).

Detailed information about V(D)J recombination and CSR will be described in the next parts.

1.3.1. V(D)J Recombination
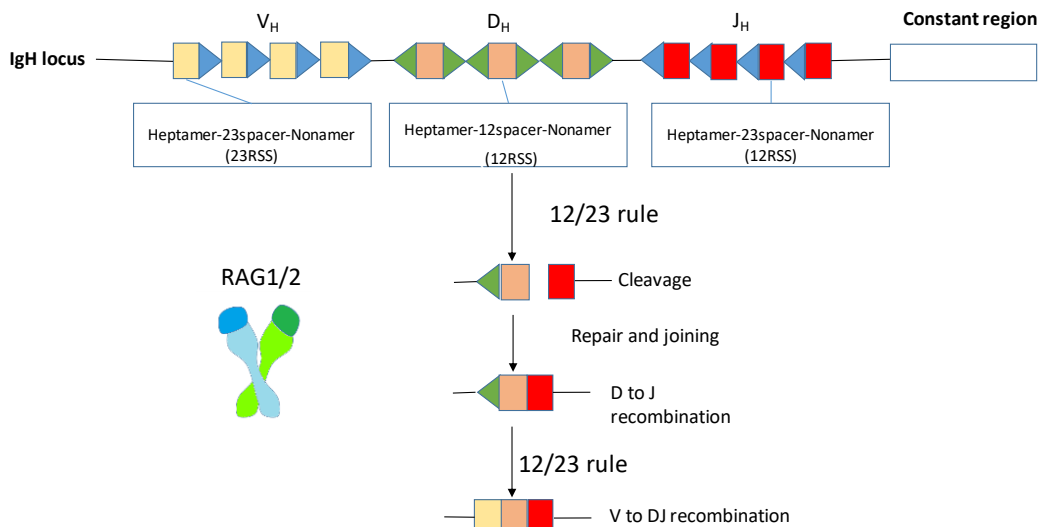
Figure 1.4. Overview of V(D)J recombination. The rectangles represent *V*, *D* or *J* segments. RAG1/2 are proteins that target and subsequently, cleave recombination signal sequence (RSS) due to 12/23 rule. *D-J* segments are recombined first and then, *V-DJ* segments are connected.

Heavy chain variable is encoded by three gene segments (*V*, *D* and *J*). During the V(D)J recombination, *D* gene segment is first joined to a *J* gene segment, then the *DJ* segment is joined to a *V* gene segment to form a complete *VDJ* exon (Arya and Bassing, 2017) (Figure 1.4).

Recombination only occurs between gene segment located on the same chromosome, and it follows the 12/23 rule stating that only a gene segment flanked by a recombination signal sequence (RSS) with a 12-base-pair spacer can be joined to one flanked by a 23bp spacer RSS. RSSs are palindromic heptamers and an AT-rich nonamer separated by spacers of 12 or 23bp. (Lina *et al*, 2016). As the result, during the rearrangement in the heavy chain, *D* gene segment can be joined to a *J* gene segment, and a *V* gene segment to a *D* gene segment but the binding of *V* gene segment to a *J* gene segment cannot be joined directly because both are flanked by 23bp spacers. However, they can be joined with the *D* gene segments between them as *D* gene segments have 12bp spacers on both sides (Murphy and Weaver, 2017).

However, the joining of *D* gene segment to another *D* gene segment still presents although it violates the 12/23 rule. This can create more diversity of antibody repertoire in the human, and this kind of antibodies represent 5% of total antibodies (Parkinson *et al*, 2015).
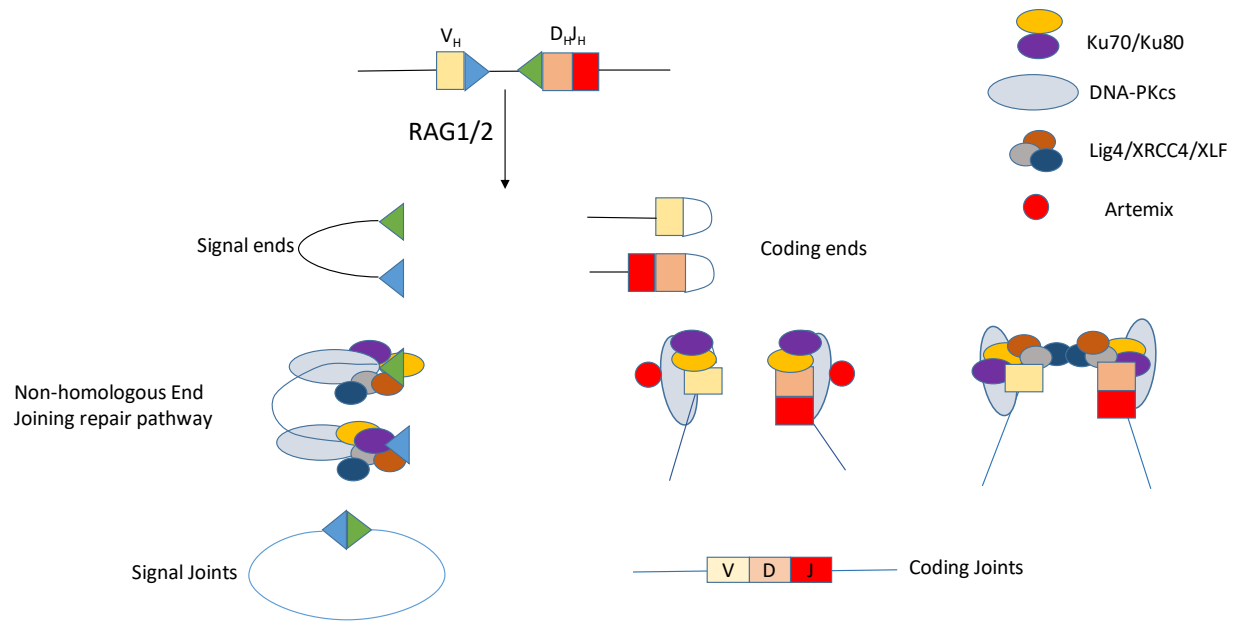
Figure 1.4. DNA repair pathway in V(D)J recombination. The solid and open triangles represent 12- and 23-bp RSSs, respectively. RAG cleaves DNA and subsequent processing and joining via NHEJ pathway occur. Ku70 and Ku80 bind to the broken DNA ends. DNA-PKcs and Artemis facilitate the opening and processing of hairpin-sealed coding ends. XRCC4 and Lig4 heterodimer seals the blunt signal ends and processed coding ends.

To initiate V(D)J recombination, the participation of RAG1 and RAG2 protein – Recombination-activating genes are required to cleave DNA at the dedicated sites. At the beginning, two RAG protein complexes recognize and align the two RSSs that are guiding the join. The RAG1 is thought to recognize the nonamer of RSS (Yin *et al*, 2009). The endonuclease activity of the RAG protein complexes makes two single-strand DNA breaks at the 5' ends- and leave the free 3'-OH group at the end of each coding segment. This 3'-OH group then hydrolyzes the phosphodiester bond on the other strand, sealing the end of the double-stranded DNA to make a DNA 'hairpin' out of the gene segment coding region. This can create the double-strand breaks at the ends of the two heptamer signal sequences (Rommel *et al,* 2017). The two RSSs are precisely joined to form the signal joint. Coding joint formation is initiated by the opening of DNA hairpin nick by a single-stranded break (Figure 1.5).

1.3.2. Class Switch Recombination (CSR)
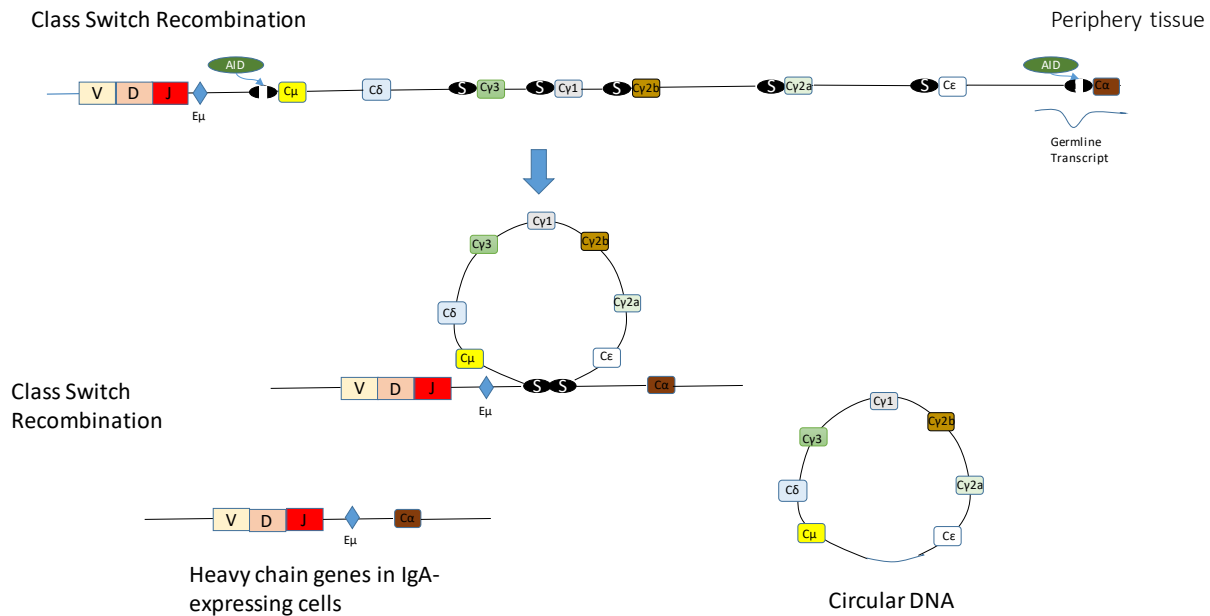
Figure 1.6. Overview of CSR. The V_H gene segments are depicted as light pink rectangles, D_H gene segments are pink rectangles and J_H gene segment are red rectangles. The *S region* exons are shown as black oval and *constant region* exons are shown rectangles that are on the right-hand side of *S regions*. The position of *Eμ* is indicated as diamond. AID is indicated as green oval. AID deaminates the *Sμ* and *Sα* regions, leading to DSBs. These regions are recombined again by a deletion recombination, which causes the expressed *V(D)J* segment to become associated with the *Cα* gene.

The consequence of successful V(D)J recombination of IgH and IgL chains in developing B cells is the surface expression of IgM or IgD, which is the signal that the immature B cells will move from the bone marrow to other lymphoid tissues to start new developmental stage, class switch recombination (CSR) (Figure 1.6). After the activation of B cells, the class switching occurs which leads in turn to the expression of IgG, IgE and IgA. As the result, this activity improves the chance of antibodies to remove the pathogen that may cause the humoral immune response. B cells can switch to any isotype and this can be directed by the induction of transcription across the S regions. Transcription promoters are located upstream the *S regions*. These promoters are activated by cytokines that induce CSR to that specific isotype. CSR is the process specific for mature B-cells.

CSR is a deletional DNA recombination occurring between *switch (S) regions*, which are located upstream of all the C_H genes except *Cδ*. Recombination occurs between two *S regions* in which DSBs are introduced on purpose: the donor *Sμ region* and an acceptor *S region* located from 65 to 160 kb downstream, although occasionally downstream *S regions* can subsequently recombine with a *S region* further downstream. *S regions* of most vertebrates are rich in G and C nucleotides, with a bias for purine nucleotides on the non-template strand of DNA (Fazzio, 2016). In addition, it also has a high density of WGCW (A/T-G-C-A/T) motifs. Such properties have been shown to increase the formation of RNA-DNA hybrids that could lead to the formation of structures such as R loops – the target of Activation-Induced Cytidine Deaminase (AID) which initiates the recombination (Bahjat and Guikema, 2017).

AID converts dC to dU residues via the hydrolytic removal of the amino group at the fourth position of the pyrimidine ring of cytidine. Deamination of dC residues by AID induces dU/dG mismatches in DNA. Subsequently, enzymes of BER and MMR pathways convert the dU's to DSBs (Okazaki, Honjo *et al,* 2002; Budzko *et al,* 2017). Uracil, whether due to the AID activity or result from the hydrolysis of cytosine, can be excised by the BER enzyme uracil DNA glycosylase (UNG), which leaves a basic (apyrimidinic, apurinic) (AP) site. AP sites are subsequently cut by AP endonuclease, APE1 and/or APE2, creating a SSB. If SSBs are sufficiently near each other on both DNA strands, DSBs are produced. The DSBs are subsequently recombined by NHEJ.
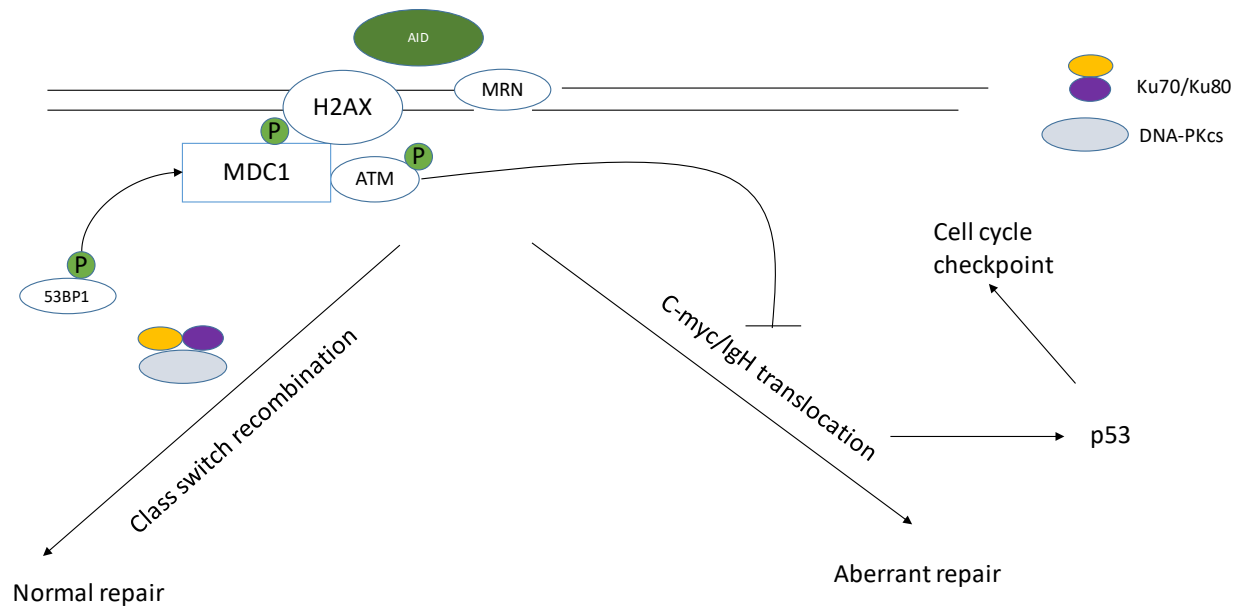
Figure 1.7. DNA repair pathways in in CSR. AID-induced DNA lesions are repaired by NHEJ factors including Ku70/80, DNA-PKcs, XLF, PAXX, Artemis, XRCC4 and Lig4. DSBs also initiate DNA damage response which includes MRN, ATM, H2AX, MDC1 and 53BP1. Failure to activate DNA repair pathway will activate p53, resulting in checkpoint arrest and cell death.

S-S recombination occurs by NHEJ, which involves binding of the abundant toroidal heterodimer Ku70/Ku80 to each DSB, forming a platform for nucleases Artemis and PALF, and for DNA polymerases, and greatly stimulating the ligation activity of DNA Lig4-XRCC4-XLF (Lobrich and Jeggo, 2017) (Figure 1.7). The Mre11-Nbs1-Rad50 (MRN) complex also rapidly binds DSBs, but it is unclear whether Ku and MRN compete or cooperate at S region DSBs. Rad50 has a long coiled-coil domain with a hook at the end by which MRN complexes bound at different DSBs can interact and tether the DSBs to each other. MRN recruits additional factors, including the kinase ataxia-telangiectasia-mutated (ATM), which activates and coordinates the cellular response to DSBs. Ku and MRN have both been shown to bind S region DSBs and contribute to CSR. ATM kinase is a major regulator of the DNA damage response and as explained above in the DNA damage response part (Brother and Attikum, 2018).

1.4. DNA damage response (DDR)
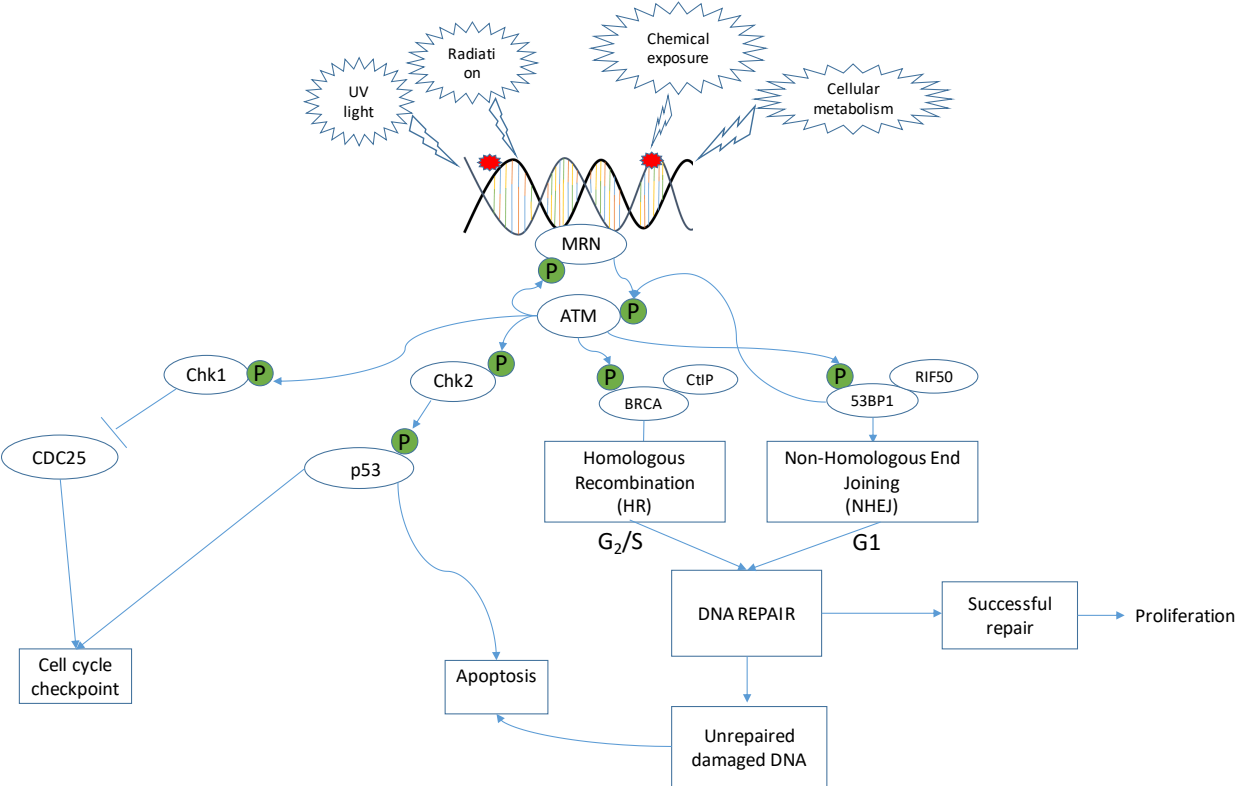
Figure 1.8. Overview of DDR. Exogeneous and endogenous factors caused the damages on DNA which triggers the DDR. In mammals, MRN complex has been proposed as sensors of DNA damage. This complex also recruits ATM which phosphorylates several downstream proteins including CHK1, CHK2, BRCA, 53BP1, p53 and CDC25 activating their functions. This phosphorylation results in different outcomes such as choices of DNA repair pathway or apoptosis.

To counteract the effects given by the DNA alterations, cells activate the DNA damage response (DDR) pathway including the detection of DNA lesion, signaling of the presence of a DNA lesion, promotion of the repair and the resolution of DNA replication issues (Figure 1.8). DDR includes post-translational modifications such as phosphorylation, ubiquitination and acetylation.

The DDR pathway was performed by phosphatidylinositol – 3 – kinase – related kinases (PIKK) including DNA-protein kinase catalytic subunit (DNA-PKcs), ataxia telangiectasia-mutated (ATM) as well as ATM and Rad3-related (ATR) (Imseng *et al,* 2018). ATM is a serine/threonine protein kinase that plays the central role in the DSB repair. Mutations in ATM cause the genetic disorder ataxia-telangiectasia (A-T), which is described by progressive cerebellar ataxia and immune deficiencies. This kinase can be recruited to the damaged site by the MRN complex

(MRE11/RAD50/NBS1). NBS1 in the MRN complex interacting with the ATM, and it helps to control the nuclear localization of MRE11 and RAD50. The MRN facilitates the activation of ATM and increases the affinity of ATM to the DDR proteins. Additionally, mediator of DNA damage checkpoint protein 1 (MDC1) recruits additional ATM molecules to DSB sites, both directly and indirectly to form the positive feedback loop (Coster and Goldberg, 2010).

After being induced by DSB, ATM is activated and this activation can be performed by post-translational modification such as phosphorylation. Autophosphorylation on Serine 1981 (S1981ph) leads to the activation of ATM by dissociation of inactivated ATM dimers (Sun *et al*, 2013). The activated ATM phosphorylates several downstream substrates, including H2AX.

H2AX is the integral part of nucleosome and it constitutes 10-15% of the histone H2A pool. It is phosphorylated by ATM, ATR and DNA-PKcs on S130 to form γ-H2AX. This histone phosphorylation acts as a docking site for DNA damage/repair proteins and functions to promote DSB repair and genomic stability (Brother and Attikum, 2018). Then, the mediator protein MDC1 is recruited to DSB sites and binds to γ-H2AX, where it further increases the accumulation of ATM (Coster and Goldberg, 2010). This forms the positive feedback loop, and it helps to spread the γ-H2AX bi-directionally from the DSBs. As the results, this relationship between MDC1, ATM and γ-H2AX increases the accumulation of repair factors. Although it might have the important role in recruiting DSB repair factors, γ-H2AX is not essential for DNA repair (Brother and Attikum, 2018).

E3 ubiquitin-protein ligase ring finger protein 8 (RNF8) is also recruited to the DSBs sites. This recruitment is facilitated by the H2AX and MDC1 through the phosphor-specific manner. The interaction between RNF8 and MDC1 will not be established unless DNA damage is induced. After being recruited to the damaged sites, RNF8 mediates the chromatin decondensation (Chitale and Richly, 2017). In addition, RNF8 performs the ubiquitylation on H2A. This ubiquitin conjugates at damaged sites act as binding sites for recruitment of several downstream factors such as BRCA1 and 53BP1 (Paul and Wang, 2017).

In addition, another positive feedback loop was also developed. When ATM phosphorylates H2AX on serine 139 to form γ-H2AX, this phosphorylation also triggers the acetylation on H3 by two histone acetyltransferases GCN5 and PCAF. Then, the chromatin remodeling complex SWI/SNF is also recruited to the damaged sites and bind to γ-H2AX through acetylated H3.

Furthermore, SWI/SNF also increases the recruitment of ATM to phosphorylate H2AX (Lee *et al,* 2010). The recent publication also confirmed the necessity of GCN5 recruitment for the efficient ATM stabilization (Salunkhe *et al,* 2018). Taken together, this forms the positive feedback loop to increase the signaling cascade in damaged sites.

ATM also helps to regulate the cell cycle arrest that gives adequate time for DNA repair as well as triggers apoptosis via phosphorylation of transcription tumor suppressor factor p53 (Ma *et al,* 2017).

1.5. GCN5 and PCAF

Among the discovered HAT, GCN5 (837 aa, 98kDa protein) was the first found as a protein for biosynthesis in yeast. Together with PCAF (832 aa, 99kDa protein), GCN5 acts as a core subunit of several HAT complexes such as SAGA, ADA and SLIK (SAGA-LIKE) or SALSA (SAGA-altered). GCN5 and PCAF can acetylate N-terminal lysine residue of histones H2B (K11/16) and H3 (K9/14/18/23/27). In addition, these acetyltransferases can also acetylate tumor suppressor factor p53. Typically, PCAF acetylates K320 which promotes the p53-dependent p21 transcription and cell cycle arrest after DNA damage. Both histone acetyltransferases belong to GCN5-related-N acetyltransferase (GNAT) superfamily. Members of this family have the conserved C-terminal bromodomain, which has been shown to be an acetyl-lysine targeting motif. Thus, a loss of its activity can lead to defects in chromatin structure and meiotic arrest (Cai *et al*, 2018).

To perform the acetyl-transfer process, there are two distinct pathways have been developed. The ping-pong mechanism at which the acetyl group is transiently attached to the enzyme and then, transferred to substrate. The other one is sequential mechanism that facilitates the direct acetyl-transfer from acetyl-CoA to the amine acceptor. This latter mechanism is also the mean by which GCN5 and PCAF can exert their functions (Jiang *et al*, 2012).

PCAF occurs in a stable multi-subunit complex containing more than 20 distinct polypeptides (Yamauchi *et al*, 2000). The characterization of subunits of the PCAF complex demonstrated that they were TATA-box binding protein associated factors which were found in transcription factor II D that bind to the TATA box in the core promoter of the gene (Ranallo *et al*, 1999).

Furthermore, GCN5 and PCAF were shown to be involved in DNA damage response. Typically, ATM phosphorylates the histone H2A on the serine 139 (S139ph) and establishes low level of γ-H2AX at the chromatin that locates around the DSBs leading to the stimulation of H3 acetylation by recruiting histone acetyltransferases GCN5 to these nucleosomes. The interaction of SWI/SNF chromatin remodeling complex to these acetylated H3 pave a way for binding to γ-H2AX. This recruitment of SWI/SNF facilitates the ATM-mediated S139ph. These events continue to form a positive feedback loop in the DNA damage response pathway (Lee *et al*, 2010). Thus, GCN5 and PCAF can be considered as the DNA damage response factors.

Previous studies showed that the deletion of *Gcn5* in mice leads to the embryonic lethality indicating the importance of this gene during the development (Yamauchi *et al,* 2000; Xu *et al*, 2000). *Gcn5*^{-/-} embryos develop normally to 10.5 days post coitum (p.t.c) and they fail to form dorsal mesoderm lineages (Yamauchi *et al,* 2000; Xu *et al,* 2000). This loss can be explained due to the increasing chance of apoptosis before the onset of morphological abnormality. In contrast, the mice carrying gene inactivating mutation of *Pcaf* are still viable with no obvious abnormalities (Yamauchi *et al,* 2000). However, compared to single knockout *Gcn5*^{-/-} and *Pcaf*^{+/-} mice, *Gcn5*^{-/-} *Pcaf*^{+/-} mice die much earlier at 7.5 p.t.c (Xu *et al,* 2000). This indicates that PCAF might contribute to some early developmental processes and the function of these histone acetyltransferases are overlapped during the embryogenesis (Yamauchi *et al¸* 2000). Furthermore, another study also indicated that deletion of *Gcn5* in mice leads to the early embryonic lethality due to increased apoptosis. When *p53* was deleted, *Gcn5*^{-/-} mice survived longer, but *p53*^{-/-}*Gcn5*^{-/-} mice still died in midgestation. In addition, to determine whether Gcn5 acetyltransferase activity is necessary during mouse development, mice carrying mutations in Gcn5 catalytic center were generated, called *Gcn5*[hat/hat]. Compared to *Gcn5*^{-/-} embryos, *Gcn5*[hat/hat] embryos did not lead to increased apoptosis but it lead to several neural tube closure defects. Taken together, *Gcn5* has important, HAT-independent function in the early development and the acetyltransferase activity is required for neural tube closure in mouse (Bu *et al*, 2007).

In addition to the above-mentioned functions, *GCN5* also participates in the regulation of IgM heavy chain gene expression. IgM proteins are present in the membrane-bound form to make up the B cell receptor and secreted form to act as soluble antibody. Deletion of this histone acetyltransferases showed the decrease in the number of membrane-bound form of IgM proteins as well as the amounts of secreted form of IgM heavy chain and light chains. Furthermore, this deletion also caused the decreased of acetylation level of H3K9 residues but not H3K14. It was consistent with several studies showing that the main substrate of *GCN5* was H3K9 ((Kikuchi *et al,* 2005; Jin *et al,* 2011). Taken together, *GCN5* is probably involved in the transcription regulation of IgM heavy chain in immature B cells (Church *et al,* 2017).

Furthermore, GCN5 and PCAF may play roles in the CSR. As mentioned in the Introduction part, CSR is initiated by AID to deaminate deoxycytidines in S regions, in 5'-AGCT-3' repeat to yield deoxyuracil (dUs). In addition to providing substrate for AID, the 5'-AGCT'-3' which is bound

by 14-3-3 adaptors, acts as anchor to organize the CSR machinery on S regions. In addition, combined histone modification in S region (H3K9acS10ph – acetylation H3 on Lysine 9 and phosphorylation on serine 10) may play a role in the targeting the CSR machinery by directly recruiting CSR factors. In 2014, Li and colleagues showed that inhibitions of enzymatic activity of GCN5 and PCAF, which performed the H3K9acS10ph, inhibits the recruitment of 14-3-3 adaptors and AID to the S regions and thus, it aborts the CSR (Li *et al,* 2014).

2. OBJECTIVES

This project aims to study the roles of two acetyltransferases, GCN5 and PCAF, during B cell development, specifically during the V(D)J recombination and CSR. As mentioned previously, $Gcn5^{-/-}Pcaf^{+/-}$ mice possess early embryonic lethality (Xu *et al,* 2000; Yaumauchi *et al*, 2000). We also generated the mouse model in which *Gcn5* was conditionally inactivated (Lin *et al,* 2008) in B lineage lymphocytes by Cre recombinase expressed under the CD19 promoter (Rickert *et al*, 1997) and *Pcaf* was inactivated in all organs (Xu *et al,* 2000). Preliminary data showed that the spleen of $Gcn5^{-/-}Pcaf^{+/-}$ mice was much smaller than that of WT mice and contained very low number of mature B cells. In the blood of $Gcn5^{-/-}Pcaf^{+/-}$ mice, the proportion of mature B lymphocytes was also very low. Furthermore, the proportion of immature B cells in bone marrow of WT, $Pcaf^{+/-}$, $Gcn5^{-/-}$ and $Gcn5^{-/-}Pcaf^{+/-}$ mice were 17%, 22%, 45%, 73%, respectively (Oksenych *et al,* unpublished data). Thus, it is hypothesized that B lymphocytopenia arises since GCN5 and PCAF are required for the early stage of B cell development. In this report, I aim to determine the role of GCN5 and PCAF during B cell development can be achieved.

To answer this question, three different cell lines were used. The HAP1 cell lines were used to study GCN5 and PCAF in the human context. Characteristics of these cells in term of proliferation were investigated.

CH12F3 cell lines were used to determine the role of Gcn5 and Pcaf during CSR. I used CRISPR/Cas9-editing strategy to inactivate these genes and then, perform *in vitro* CSR. In addition, I investigated proliferation of these cells.

vAbl pro-B cells were used to study the role of acetyltransferases Gcn5 and Pcaf during V(D)J recombination. Defect in V(D)J recombination leads to the abolishment of B and T lymphocyte development resulting in several combined deficiency (SCID). CRISPR/Cas9 editing strategy was used to inactivate these genes and *in vitro* V(D)J recombination was carried out.

Inactivation of *Gcn5* and *Pcaf* genes in B lymphocytes will provide us better understanding of their roles in DNA repair, V(D)J recombination and CSR during B cell development.

3. Materials and methods

3.1. Cell lines

3.1.1. HAP1

HAP1 is an adherent human near-haploid cell line derived from the KBM-7 cell line found in a male patient with chronic myeloid leukemia, characterized by the increased and unregulated growth of myeloid cells in bone marrow and the accumulation of these cells in blood. Due to the near-haploid characteristics, these cells are ideal model for the genetic and biomedical studies. Indeed, there is only one copy of each gene, so mutated phenotypes are immediately exposed. In this study, I am using the commercially generated $GCN5^{KO}$, $PCAF^{DKO}$ and $GCN5^{KO}PCAF^{KO}$ HAP1 cells as well as parental control cells (WT) produced and provided by Horizon Discovery (Austria).

Horizon Discovery generated knockout HAP1 cells using CRISPR/Cas9 gene editing technology.

Name	Mutation
$GCN5^{KO}$ HAP1 cells	1bp insertion in exon 1
$PCAF^{KO}$ HAP1 cells	1bp insertion in exon 2
$GCN5^{KO}PCAF^{KO}$ HAP1 cells	1bp insertion in exon 1 and 1bp insertion in exon 2

Table 1. Information of modified HAP1 cell lines regarding type and position of mutation.

3.1.2. CH12F3

CH12F3 is a cellular model system to study the Class Switch Recombination (CSR) due to its ability to switch from IgM to IgA after treatment with CD40L, TGF-β and IL-4 during 72h. This cell line is available in our research group and CRISPR/Cas9 method was used to generate $Gcn5^{-/-}$ and $Pcaf^{-/-}$ cells.

CH12F3 is derived from CH12-a murine B lymphoma cell line bearing surface of the phosphatidylcholine moiety of sheep red blood cell membranes. The CH12.LX cell line is in vitro-adapted cell line derived from CH12 and contains a large population of IgM-bearing cells and small numbers of IgA-bearing cells. At the beginning, the cells had a capacity to switch to both IgG and IgA. However, the latter occurs at the low frequency (4% of cells) so the researchers continued to sub-clone these cells. Among the clones, the CH12F switched to IgA most frequently,

while the CH12D switch least frequently in the presence of cytokines. The further limited dilution gave rise to the CH12F3 clone, which became the model to study CSR (Nakamura et al, 1996).

3.1.3. vAbl

vAbl (Abelson murine leukemia virus kinase-transformed pre-B stage) murine cell lines, available in our group, carry knocked-in Eμ-*Blc2+* transgene enhancing the cell survival in G1 phase of the cell cycle while expressing RAG1/RAG2, to initiate the V(D)J recombination after treatment with the tyrosine kinase inhibitor STI-571.

Abelson murine leukemia virus was isolated in 1970 (Abelson and Rabstein, 1970). This virus expresses the v-Abl protein that induces the pre-B cell malignant transformation. The v-Abl protein is a nonreceptor tyrosine kinase that plays important role in the regulation of proliferation and differentiation of pre-B cell. This feature makes the vAbl cell suitable model to study the pre-B cell differentiation, including immunoglobulin gene rearrangement (Rosenberg et al, 1975).

This cell line is available in our research group and CRISPR/Cas9 gene editing method was used to generate the *Pcaf$^{-/-}$* vAbl cell line.

3.1.4. HEK293T

HEK293T is a human embryonic kidneys cell derived from HEK293 cell lines expressing a mutant version of SV40 T-antigen which binds to the origin region of the genome as well as tumor suppressor proteins (p53 and retinoblastoma) resulting in the entering S phase which triggers the DNA replication. Because of the high efficiency of transfection, HEK293T are widely used for retroviral production, gene overexpression and protein production.

3.1.5. Phoenix

Phoenix cells are a second-generation retrovirus producer lines. These cells were created by replacing into HEK293T cells the construct of producing gag-pol and envelop proteins. As the result, the Phoenix cells stably expressed gag-pol and envelope protein eliminating the need to deliver these genes by specific plasmids, giving the ability to produce virus in few days or hours. These cells are transfected with high efficiency using calcium phosphate medium or lipid-based transfection protocols, when up to 50% or higher proportion of cells can be transfected.

3.2. Cell culture

3.2.1. HAP1

Wild-type (WT), $GCN5^{KO}$, $PCAF^{KO}$ and $GCN5^{KO}PCAF^{KO}$ HAP1 cells were cultured in Iscove's Modified Dulbecco's Medium (IMDM) (Thermo-Fisher, 12440053) supplemented with 10% fetal bovine serum (FBS) (Thermo-Fisher, BCBQ9326V) and 1% Streptomycin/Penicillin (Thermo-fisher, 15140122), 1% L-glutamine (Thermo-fisher, 25030081) and maintained in culture at $37^{\circ}C$ in 5% CO_2 (Steri-Cycle CO_2 incubator (HEPA class 100, Thermofisher).

To keep cells in culture, medium was aspirated by vacuum machine and the cells were washed with 5mL of home-made Phosphate-buffered Saline (PBS1X) before treating with 1mL of trypsin (Sigma, SLBR9153V) per 10cm plates and incubated at $37^{\circ}C$ in 5% CO_2 for 3-5 minutes. Trypsin was neutralized by dilution in 9mL of culture medium and 1mL of suspension was transferred to the 10cm plate containing 9mL of culture medium.

To freeze the cells, medium was aspirated by vacuum machine and cells were washed with 5mL of PBS1X. One mL of trypsin per 10cm plates was added to detach the cells from surface of plates and the cells were incubated at $37^{\circ}C$, 5% CO_2 for 3-5 minutes. Trypsin was neutralized by dilution in 9mL of culture medium and all suspension was transferred to 15mL Falcon (VWR-5250604) and precipitated by centrifuge at 1500rpm for 5 minutes at room temperature (Rotina 380 hettich zentrifugen). The supernatant was discarded and cell pellets were resuspended in 3mL of freezing medium containing 10% dimethyl sulfoxide (DMSO) (Sigma, BCBS5472) and 90% of FBS. One mL of freezing medium containing cells was added into 3 CryoTubes (SARSTEDT, 72.377, CryoPure tube 1.0 ml white). The tubes were kept at $-80^{\circ}C$ for short-term storage and in liquid nitrogen for long-term storage.

To thaw the cells, I used the water bath at $37^{\circ}C$, and then 1ml of cell suspension was added directly to 10cm cell culture plate. After 24h, medium was aspirated and cells were washed by 5mL of PBS1X to remove DMSO from the cells. 10mL of culture medium was added to the 10cm plate and cells were kept in culture for 2-4 days.

3.2.2. CH12F3 and vAbl

WT, $Gcn5^{-/-}$, $Pcaf^{-/-}$, $Aid^{-/-}$ and $Ung^{-/-}$ CH12F3 as well as WT, $Pcaf^{-/-}$ and $Dna\text{-}pkcs^{-/-}Xlf^{-/-}$ vAbl cell lines were grown in Roswell Park Memorial Institute 1640 Medium (RPMI) supplemented with

10% fetal bovine serum (FBS), 1% Streptomycin/Penicillin, 1% L-glutamine, 1% Non-essential amino acid (NEAA) (Thermo-fisher, 1895809), 1% sodium pyruvate solution, (Thermo-fisher, 8636) and 0.1% β-mercaptoethanol 50nM (Gibco, 31350-010). These cell lines were maintained in culture at 37°C and 5% CO_2.

To keep the cells in culture, few drops of cell suspension was transferred to the T25 flask containing 9mL of culture medium and the cell were cultured for 3-5 days.

Cells in T25 flask were frozen by transferring into 15mL Falcon and centrifuging at 1500 rpm in room temperature during 5 minutes. The supernatant was discarded, cell pellets were washed in 5mL of PBS1X and centrifuged at 1500 rpm at room temperature during 5 minutes. The supernatant was discarded and cell pellets were resuspended in 3mL of freezing medium containing 10% of dimethyl sulfoxide (DMSO) and 90% of FBS. One milliliter of freezing medium containing cells was added into 3 cryotubes. The tubes were kept at -80°C for short-term storage and in liquid nitrogen for long-term storage.

To thaw the cells, 1mL of freezing medium was transferred to 15mL Falcon containing 4mL of culture medium and cells were centrifuged at 1500 rpm during 5 minutes at room temperature. The supernatant was discarded, 5mL of PBS1X were added to wash the cells and then, the cells were centrifuged at 1500 rpm during 5 minutes at room temperature. The supernatant was discarded, cell pellet was resuspended in 1mL of culture medium, transferred to T25 flasks containing 9mL of culture medium and cells were kept in culture.

3.2.3. Phoenix and HEK293T cells

HEK293T and Phoenix cells were cultured in Dulbecco's modified Eagle's Medium (DMEM) (Sigma Aldrich, D6046) supplemented with 10% Fetal Bovine Serum and 1% Penicillin/Streptomycin at 37°C in 5% CO_2.

Because Phoenix and HEK293T are also adherent, keeping in culture, freezing and thawing procedures were identical to those of HAP1 cells, described in part 1 of section II.

3.3. Generation of knockout cell lines by the CRISPR/Cas9 method
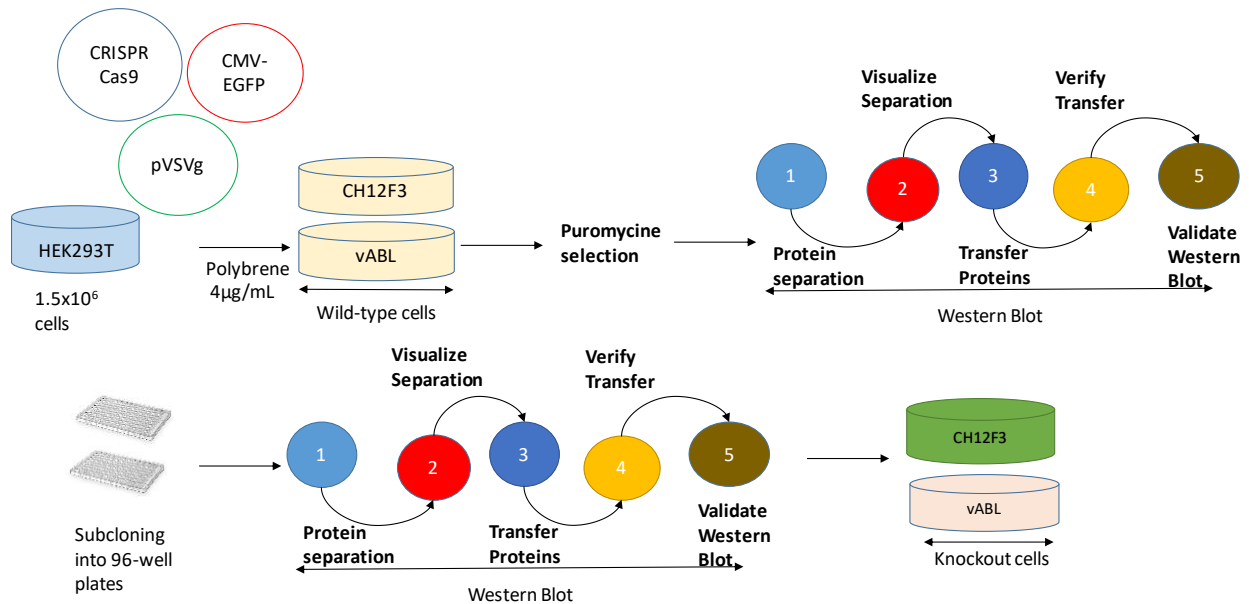
Figure 3.1. Generations of knockout CH12F3 and vAbl cells. Retroviral supernatant was produced by transfection of CRISPR/Cas9 plasmids containing specific gRNA of target genes into HEK293T cells. This supernatant was transduced to WT CH12F3 and WT vAbl cells with the aid of polybrene 4µg/mL and 24h post second transduction, puromycine selection was performed to eliminate non-transduced cells. CH12F3 and vAbl cellular pools were in culture for 2-4 days for freezing and western blot analysis. Only the pool that had the lowest protein expression level was chosen for further subcloning. Isolated clones were screened by western blot.

3.3.1. Preparation of retroviral supernatant

HEK293T cells were plated at a final concentration of $1,5 \times 10^6$ cells/mL in 6-well plates at day 0. To count the cells, 10µL of Tryptophan Blue stain 0.4% (Thermofisher, T10282) and 10µL of suspension cells were mixed onto the Countess^{TM} cell counting chamber slide (Invitrogen) and counted on the Countess^{TM} Automated Cell Counter (Invitrogen).

At day 1, retroviral supernatants were prepared by transfection of HEK293T cells with 2µg pLcV2 guide RNA sequence plasmid (Addgene) and 3µg of packaging plasmid (Thermofisher, K497500) by using FUGENE 6 DNA Transfection Reagent (Promega, E2691). Packaging plasmid contains *gag*, *pro, pol* and *env* genes. *Gag* encodes the major structural glycoprotein Gag, the viral protease

is encoded by *pro* and is responsible for the maturation of viral particles. The products of *pol* include reverse transcriptase and integrase while *env* is responsible for the viral surface that mediate the receptor binding and membrane fusion.

Forty eight hours after the transfection, the medium of HEK293T cells containing virus was added to vAbl and CH12F3 cells for the transduction as described below.

3.3.2. Transduction of vAbl and CH12F3 cells

Twenty-four hours before the transduction, 10^5 of WT vAbl pro-B cells and WT CH12F3 cells were plated into 12-well plates (SARSTEDT). Forty-eight hours after the transfection of HEK293T cells, the retroviral supernatant was filtered through the 0,45µm filter (VWR Sterile Syringe filter, 28145-481) together with a plunger (Terumo, 2.5 mL, 02SE1). The retroviral supernatant was completed to 2mL with HEK293T medium. Two microliters of polybrene (Sigma-Aldrich, TR-1003-G, stock 8µg/µL) were added to the viral supernatant to have a concentration of 8µg/mL. One mL of polybrene/virus was added to the targeted cells (vAbl and CH12F3). The final concentration of polybrene was 4µg/mL. Two milliliters of HEK293T cells were added to the cells for a second transduction of cells and incubated at 37^oC in 5% CO_2. Twenty-four hours after the first transduction, a second one was carried out as described above. Twenty-four hours after the second transduction, 1µg/mL – final concentration- of puromycine (Invitrogen, QLL-3801A) was added to each well to select cells containing the pLcV2 plasmid. After 7 days of selection, cells were amplified into T25 flasks for freezing and in 6-well plates for screening by western blot analysis described in part 4- Western blot analysis.

3.3.3. Sub-cloning

Three 96-well plates (SARSTEDT) containing 0.5 cells per well were used. vAbl and CH12F3 cells were counted using the Countess^{TM} Automated Cell counter (Invitrogen) by mixing 10µL of Tryptophan Blue stain 0.4% (Thermofisher, T10282) and 10µL of suspension cells were mixed onto the Countess^{TM} cell counting chamber slide (Invitrogen). The cells were diluted at a ratio of 1:100 first and then at a ratio of 1:10. RPMI1640 medium was transferred to the VWR reagent reservoirs (50mL disposable, Pre-Sterile, poly-styrene reservoir) and multi-channels pipette was used to transfer 150µL of cell suspension to each well of 96-well plates. Cells were incubated at 37^oC in 5% CO_2 for 7-10 days. Then, the selected clones were transferred to 12-well plates for the maintenance in culture and in 6-well plates for screening by western blot analysis.

3.3.4. Western Blot analysis

3.3.4.1. Dry cell pellets collection

Cells were transferred into a 15ml Falcon tube and precipitate by centrifugation at 1500rpm for 5 minutes at room temperature. Supernatant was discarded, cells were washed in 5mL of PBS1X and centrifuged at 1500 rpm for 5 minutes at room temperature. Supernatant was discarded, cells were suspended in 1mL of PBS1X, transferred into 1.5mL micro tube and centrifuged at 1500rpm for 5 minutes at room temperature. Supernatant was discarded and dry pellets were stored at -80°C.

3.3.4.2. Cell extractions and protein concentration measurements

For whole cell extracts, exponentially growing cells were lysed in Radioimmunoprecipitation assay buffer (RIPA) buffer containing 50mM Tris pH 8.0 (Roche, 10708976001), 150mM NaCl (Merck KGAA, 7647-14-5), 1mM EDTA (Merck KGA, 60-00-4), 1mM Pefabloc (Roche, 11429868001), 1% Triton (Sigma, MKBV8814V), 20mM Na pyrophosphate, PIC2 (Sigma Aldrich, P5726) and PIC3 (Sigma Aldrich, P0044, 1000x), 0.5% SDS (Sodium dodecyl sulfate, Sigma-Aldrich, 028K0108) and 25xPIC (Sigma Aldrich, P8340) for 30 minutes on ice. Cells were centrifuged at 13000 rpm at 4°C during 15 minutes (5424R eppendorf centrifuge with rotor FA 45 24 11). Supernatant containing whole cell extracts were transferred into a 1.5mL Eppendorf tube and protein concentrations were measured using Bradford protein assay. Briefly, 1µL of each sample and 19µL of distilled water were mixed with 1mL Protein assay dye concentrate reagent (Bio-Rad, 500006) diluted 1:5 in distilled water before used. Protein concentrations were measured at the absorbance of 595 nm using the UV-1700 Pharma Spec spectrophotometer (Shimadzu).

To ensure that the measurement of protein concentration was precise, Bovine Serum Albumin (BSA) (Sigma, SLBS1213V) of known concentration was used as standard curve. The specific information about used volumes are described in the table below.

Cuves	0	1	2	3	4	5	6
BSA (µg)	0	0	2	4	10	14	22
BSA (2µg/µl) (µL)	0	0	1	2	5	7	11
H$_2$O (µL)	20	20	19	18	15	13	9
Bradford reagent (µL)	1000						

Table 2. Preparation of BSA standard curve.

For acid extracts, cell pellets were resuspended in 200µL of TEB (Triton Extraction Buffer) buffer containing 250µL Triton, 0.5%, 5µL Pefabloc 1mM; 10µL NaN3, 0.02 %; and 4735µL PBS1X. Samples were incubated on ice for 10 minutes and centrifuged at 8000 rpm at 4°C for 5 minutes. Cell pellets were washed in 100µL of TEB buffer and centrifuged at 8000rpm at 4°C for 10 minutes. Supernatants were removed, cell pellets were resuspended in 100µL of 0.2N HCl/PBS (19.7µL of 37% HCl (VWR Chemicals, 16J124012) into 1mL of PBS1X), incubated at 4°C overnight and centrifuged at 8000rpm at 4°C for 5 minutes. Supernatants were transferred into 1.5mL Eppendorf tubes and used as acid extracts. Protein concentrations were quantified by Bradford protein assay as described for the whole cell extracts.

3.3.4.3. Electrophoresis, transfer and membrane picture

Equivalent amount of proteins was analyzed by SDS-PAGE. Typically, for whole cell extracts, 35 to 50µg of proteins were used. For acid extracts, 10µg were used to analyze H3K9ac and H3K14ac, and 1µg was used to analyze H3.

First, equivalent amount of proteins was mixed with 1µL of Dithiothreitol (DTT, 10mM, Thermofisher, R0861), 2,5 or 5µL of Lithium Dodecyl Sulfate (LDS) NuPAGE loading buffer (Thermofisher, NP007) and distilled water for a final volume of 3µL or 20µL, respectively. Samples were vortexed and quickly spun down. Then samples were incubated at 70°C for 10 minutes to denaturate higher order structure of protein, vortexed and quickly spun down.

Five microliters of Seeplus stain (Invitrogen, LC5925) and 3µL of Magic Marker stain (Invitrogen, LC5602) together with 4µL of distilled water were mixed to form the protein ladders. Seeplus stain

was used to visualize the molecular weight of protein during electrophoresis. Magic marker stain was designed to estimate the molecular weight directly on Western Blot.

Samples were loaded in NuPAGE[tm] Bis-Tris 4-12% gel, 1.0 mm, 12-well or 10-well (Invitrogen, NP0321) and migration was performed in the XCell SureLock Minicells (Thermofisher) containing the running buffer NuPAGE[tm] MOPS (Invitrogen). Gel electrophoresis was performed at 200V during 45 minutes.

Proteins were transferred on hydrophobic PVDF (polyvinylidene fluoride) Immobilon transfer membranes, pore size (0.2nm) (Invitrogen, ISEQ26260). Prior protein transfer, the membrane was activated by soaking it into 100% methanol (Fisher Chemical, 1737138) for 2 minutes, washed in water for 2 minutes and soaked in transfer buffer (1X) containing 50mL NuPAGE[tm] transfer buffer (20x, Thermofisher, NP0006), 850mL of distilled water and 100mL of 100% methanol for 5 minutes, to equilibrate the membrane.

For the transfer, a western blot "sandwich" was prepared. It consisted of filter papers (Sigma-Aldrich, WHA10538010), gel and equilibrated membrane. The "sandwich" was placed into the transfer tank containing the transfer buffer. Electroblotting was performed at 25V during 90 minutes at +4°C.

Membranes were then washed quickly in PBS 1X-0.1% Tween20 (PBS-T) and blocked in 5% skimmed milk in PBS-T (PBS-T- milk) during 1h under agitation (20rpm, Lab companion SK-300 dual action shaker). Then, membranes were washed in PBS-T three times for 10 minutes under agitation and incubated with primary antibodies overnight at 4°C, under agitation (see table 1). On the next day, membranes were washed in PBS-T three times for 10 minutes under agitation and incubated with horseradish peroxidase-conjugated anti-mouse or anti-rabbit secondary antibodies for 2h at room temperature (see table 1) under agitation. Membranes were washed with PBS-T three times for 10 minutes under agitation and reviewed using Kodak image software in the Kodak Image station 4000R using 1mL of Super Signal West Femto maximum sensitivity substrate (Thermofisher. 34095) to trigger the chemiluminescence reaction. The detail information of antibodies is mentioned in the table below.

Name	Species	Dilution	Solution	Company
PCAF	Rabbit	1:1000	PBS-T 0.1% + 5% BSA	Cell signaling
Gcn5	Mouse	1:2000	PBS-T 0.1% + 5% milk	Abcam
H3K9ac	Rabbit	1:500	PBS-T 0.1% + 5% milk	Abcam
H3K14ac	Rabbit	1:1000	PBS-T 0.1% + 5% milk	Millipore
H3	Rabbit	1:2000	PBS-T 0.1% + 5% milk	Abcam
Actin	Mouse	1:2000	PBS-T 0.1% + 5% milk	Abcam
Polyclonal rabbit @-mouse	Rabbit	1:2000	PBS-T 0.1% + 5% milk	Dako
Polyclonal swine @-rabbit	Swine	1:2000	PBS-T 0.1% + 5% milk	Dako

Table 3. List of antibodies used for western blot analysis.

3.4. Proliferation assay

To perform proliferation assay, 10^5 of WT, $GCN5^{KO}$, $PCAF^{KO}$ and $GCN5^{KO}PCAF^{KO}$ HAP1 cells were plated in triplicate in 6-well plates at day 0. The cells were counted at days 1, 2, 3 and 4. Specifically, 10μL of Tryptophan Blue stain 0.4% (Thermofisher, T10282) and 10μL of suspension cells were mixed onto the Countess^{TM} cell counting chamber slide (Invitrogen) and counted on the Countess^{TM} Automated Cell Counter (Invitrogen).

In addition, 7×10^4 of WT, $Gcn5^{-/-}$ and $Pcaf^{-/-}$ CH12F3 cells were plated in triplicate in 6-well plates at day 0. Cells were counted at days 2, 3 and 4. Specifically, 10μL of Tryptophan Blue stain 0.4% (Thermofisher, T10282) and 10μL of suspension cells were mixed onto the Countess^{TM} cell

counting chamber slide (Invitrogen) and counted on the Countess[TM] Automated Cell Counter (Invitrogen).

3.5. Cell cycle analysis

To analyze distribution of cells through the cell cycle, 10^6 WT, *GCN5^{KO}*, *PCAF^{KO}* and *GCN5^{KO}PCAF^{KO}* HAP1 cells were centrifuged at 6000rpm at 4°C during 5 minutes. The supernatant was discarded and the cells were resuspended in 100μL of PBS1X. One milliliter of ice cold methanol was added to the cell suspension, mixed by vortex and stored at -20°C until analysis. Methanol was used to permeabilize the cells sufficiently to label with chemical dye.

On the day of analysis, the cells were centrifuged at 5000rpm during 5 minutes at 4°C, supernatants were discarded and the cells were washed in 750μL of PBS1X. The cells were resuspended in 200μL of 0.1mg/mL RNAse A (Thermofisher, EN0531, in PBS1X) and incubated at 37°C for 30 minutes to eliminate RNA present in the cells. Then, propidium iodide (1mg/mL, Sigma-Aldrich, MKBV9923V) was added to cells for the collection of dead cells and incubated for 30 minutes at 37°C. The samples were kept on ice until the cell cycle analysis. The analysis was performed on the BD FACS_Canto machine and analyzed by BDFACSDIVA[TM] software. Further analysis of results was performed using the FlowJo software (FlowJo LLC).

3.6. V(D)J recombination

3.6.1. Production of virus

On the first day of experiment, $1,5x10^6$ of Phoenix cells were plated in 10cm plates (SARSTEDT). Twenty-four hours later, the cells were transfected with 1.4μg of V(D)J recombination plasmid, pMX-INV and 0.9μg of pCL EcoR helper plasmid using the FUGENE 6 DNA Transfection Reagent to a ratio 2:1 (Promega, E2691) according to the manufacture's protocol. The incubation was performed at 37°C in 5% CO_2 during 48h.

pMX-INV has a single pair of recombination signals that flank an antisense green fluorescence protein (GFP) cDNA and perform the recombination by inversion. So, the normal rearrangement will place the cDNA in the sense orientation leading to the GFP expression (Bredemeyer et al, 2006). pCL EcoR helper plasmid is one of three members belonging to the pCL packaging plasmid family that express high levels of *gag*, *pol*¸and *env* proteins. This pCL-EcoR produces the

ecotropic viruses that are suitable for infection of mouse cells, in this case, vAbl murine pro-B cells. The efficiency makes this plasmid a convenient way to produce the helper-free recombinant retrovirus (Naviaux et al, 1996).

After the transfection, the medium of Phoenix cells containing the virus was added to the vAbl and CH12F3 cells for the transduction of virus, as described in section 2.

3.6.2. Transduction of vAbl cells

Twenty four hours before the transduction, 10^5 of WT, *Pcaf$^{-/-}$* and *Dna-Pkcs$^{-/-}$/Xlf$^{-/-}$* vAbl pro-B cells were plated into 12-well plates (SARSTEDT). Fourty eight hours h after the transfection of Phoenix cells, the retroviral supernatant was filtered using a 0,45µm filter (VWR Sterile Syringe filter, 28145-481) together with a plunger (Terumo, 2.5 mL, 02SE1). The retroviral supernatant was completed to 2mL with Phoenix medium. Two microliters of polybrene (Sigma-Aldrich, TR-1003-G, stock 8µg/µL) was added to the viral supernatant to have a final concentration of 8µg/mL. One milliliter of polybrene/virus mixture was added to vAbl cells. The final concentration of polybrene was 4µg/mL. Two milliliters of Phoenix cells were added to the cells for a second transduction of cells and the cells were incubated at 37°C in 5% CO_2. vAbl cells in 12-well plates were then centrifuged at 1800rpm for 75 minutes at room temperature. Twenty four hours after the first transduction, a second transduction was carried out as described above.

3.6.3. Purification of hCD4+ containing cells

vAbl pro-B cells were then enriched based on the human CD4 (hCD4) marker expression using hCD4 Microbeads (MACS Miltenyi Biotec, 5151216402), according to the manufacturer instructions. Typically, 10^7 of pro-B cells were washed in cold filtered buffer containing 0.5% BSA, 2mM EDTA, PBS1X pH 7.2. After centrifugation at 1800 rpm for 10 minutes at 4°C, supernatants were removed and cell pellets were resuspended in 80µL of buffer. Then, 20µL of hCD4 Microbeads were added and incubated for 15 minutes in the refrigerator. Further, the cells were washed in 1mL of buffer and centrifuged at 1800 rpm for 10 minutes at 4°C. Supernatants were aspirated completely and pellets were suspended in 500µL of buffer before magnetic selection using MS Column (Miltenyi Biotec, 130042201) and MACS MultiStand (Miltenyi Biotec). To perform the selection, 500µL of buffer were used to remove the hydrophilic coat of the column; this step was performed 3 times. Then, cell suspensions were applied onto the columns. The unlabeled cells were collected in BD Falcon Conical tubes by washing the columns

three times with 500µL each time. The buffer was added only when the column reservoir was empty. Then, MS columns were removed from the MACS MultiStand and placed them onto another suitable BD Falcon Conical tube. 1mL of buffer was added onto the MS Column and immediately flushed out fraction with the magnetically labelled cells by firmly pushing the plunger into the column. All steps in this procedure were performed on ice.

Then, WT, $Pcaf^{-/-}$ and $Dna\text{-}Pkcs^{-/-}Xlf^{-/-}$ vAbl cells were transferred to 1.5mL Eppendorf tubes and centrifuged at 4ºC at 1800rpm during 10minutes. Supernatants were discarded and cells were suspended in 1mL of culture medium RPMI1640, transferred to a 6-well plate and maintained in culture for four days until the STI-571 treatment.

3.6.4. STI-571 treatment and FACS analysis

After four days in culture, 10^6 of WT, $Pcaf^{-/-}$ and $Dna\text{-}Pkcs^{-/-}Xlf^{-/-}$ of pMX-INV vAbl pro-B cells were plated in 6-well plates and treated with 3µM of vAbl tyrosine kinase inhibitor Imatinib STI-571 (Sigma-Aldrich, PD180970, 10mg/mL) during 96h to stop the cell cycle in G1 phase and to induce the expression of RAG1/RAG2 initiating the V(D)J recombination. Cells were analyzed for recombination levels by FACS analysis of GFP/hCD4 expression. For that, pMX-INV vAbl-enriched pro-B cells were transferred to a 1.5mL Eppendorf tube and centrifuged at 1500rpm at 4ºC during 5 minutes. Supernatants were discarded and the cells were washed twice with 1mL of cold PBS1X. The cells were then resuspended in 100µL of cold PBS1X, 5µL of hCD4-PE antibody (Invitrogen, 12004942) was added to the cell suspension and incubated on ice in the dark during 30 minutes. Cells were washed twice in 1mL of cold PBS1X and centrifuged at 1500rpm at 4ºC for 5 minutes. Supernatant was discarded, cell pellets were resuspended in 500µL of PBS1X and transferred to the BD Falcon Conical tubes. All steps in this procedure were performed on ice. The analysis was performed on the BD FACS_Canto machine and analyzed by BD FACSDIVA™ software. Further analysis of results was performed using the FlowJo® software (FlowJo LLC).

3.7. **Class Switch Recombination assay**

WT, $Gcn5^{-/-}$(clone 3)*, $Pcaf^{-/-}$(clone 34)*, $Aid^{-/-}$ and $Ung^{-/-}$ CH12F3 cells were plated at a final concentration of 10^4 cells/mL in 96 well plates. $Aid^{-/-}$ and $Ung^{-/-}$ CH12F3 cells from the lab of Bodil Kavli were used as negative controls. These cells were deficient in AID and UNG, respectively which are both essential for initiation of class switch recombination (Dewan *et al*,

2018). One hundred microliters of medium were added to each well in quadruplicate for unstimulated and stimulated cells. For the unstimulated cells, 100µL of culture media was added while in the wells containing stimulated cells, 100µL stimulation mixture containing IL-4 (5µg/mL, PeProtech, 2141420UG), TGF-β (10µg/mL, Peprotech, 100-21-100UG), CD40L (1µg/mL, BD Biosciences, 553721) was added to each well. Cells were incubated in 96h at 37°C in 5% CO_2.

For analysis, four wells from the same samples were transferred to one Eppendorf tube and centrifuged at 5000rpm at 4°C during 5 minutes. Supernatant was discarded, cell pellets were resuspended in PBS1X and centrifuged at 5000rpm at 4°C during 3 minutes. Cell pellets were resuspended in 150µL of live/dead solution (1:1000 in PBS, LifeTechnology, 10120) and incubated at 4°C for 15 minutes in the dark. Then, 50µL of FcBlock buffer (BD purified rat α-mouse CD16/CD32, 1:50 in PBS, BD Biosciences, 553141) were added to each sample and incubated at 4°C for 15 minutes in the dark centrifuged at 5000rpm at 4°C during 3 minutes. Supernatant was discarded and cell pellets were washed with PBS, resuspended in 200µl BD Cytofix/Cytoperm (BD Biosciences, 20015Z) and incubated at 4°C for 30 minutes in the dark. Then, the cells were washed in 150µL of cold Permwash (1:10 cytofix/cytoperm wash in sterile H_2O, BD Biosciences, 51-2091KZ), resuspended in 50µL antibody solution (α-mouse IgA PE 0,1 mg/ml, 1:200 in Permwash, BD Biosciences, 12-5944-81), incubated at 4°C for 30 minutes in the dark. 100µL Permwash was added to each sample and the cells were centrifuged at 5000rpm at 4°C during 5 minutes. Then, the cells were resuspended in 100µL PBS and transferred into BD Falcon Conical tubes containing 200µL PBS1X. The analysis was performed on the BD FACS_Canto machine and analyzed by BD FACSDIVA^{TM} software. Further analysis of results was performed using the FlowJo® software (FlowJo LLC).

4. Results

4.1. HAP1

4.1.1. Verification of *GCN5* and *PCAF* inactivation
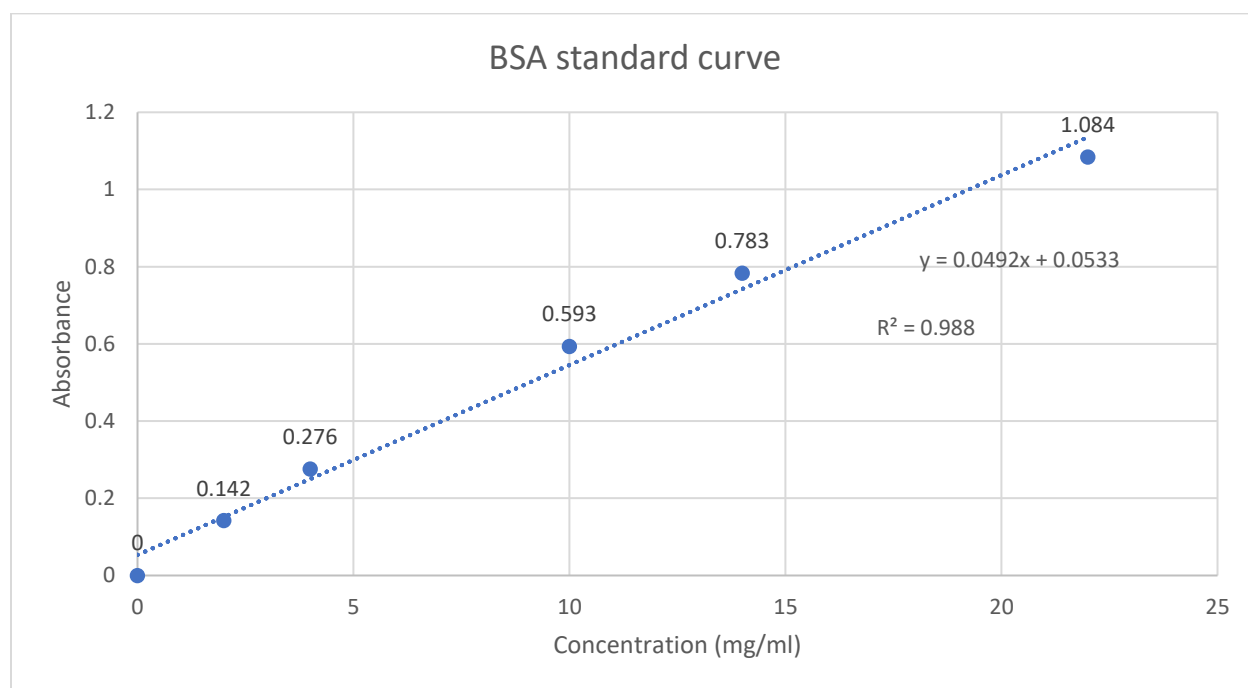
Figure 4.1. Example of standard curve resulting from measuring concentrations of BSA.
BioRad Bradford reagents and Shimadzu Spectrophotometer were used to perform this analysis. Six standards were used for generating the standard curve that covered expected range of unknown samples. The absorbance was measured at 595nm.

To measure the protein concentration, the standard curve was made first. In this linear model, I calculated the coefficient of determination to estimate how well the data fit the standard. R^2 is a measure of percentage of total variation in the dependent variable (concentration) that is accounted for the independent variable (absorbance) (Hamilton *et al*, 2015). Typically, Figure 4.1 showed that R^2 was 0.988, which means that nearly 99% of the variability in the outcome data could be explained by the model. To conclude, this experiment increased the accuracy of measurement of protein concentration.
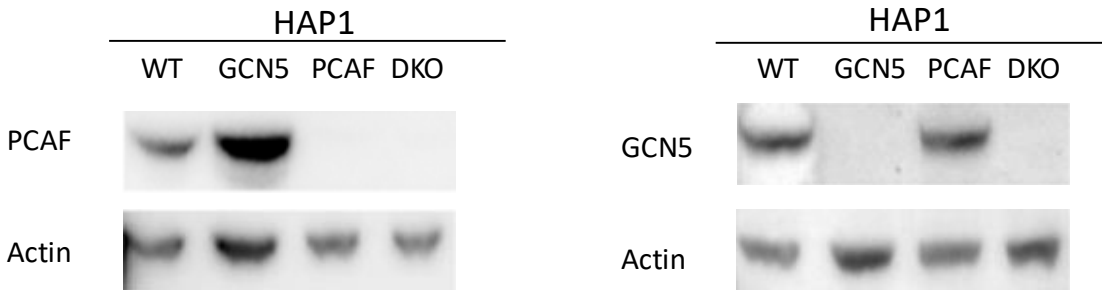
Figure 4.2. Determination of protein expression levels of PCAF and GCN5 in HAP1 cells by western blot. The level of actin was also checked by monoclonal anti-actin antibody as internal control. Equal amounts of cell extracts were run on SDS-PAGE before immunoblotting.

The abolishment of GCN5 and PCAF proteins in $GCN5^{KO}$, $PCAF^{KO}$ and $GCN5^{KO}PCAF^{KO}$ HAP1 cells was confirmed by western blot. As shown in Figure 4.2, there was no PCAF protein expression in $PCAF^{KO}$ HAP1 cell indicating that the deletion of this protein was successful compared to WT HAP1 cell. Similarly, no GCN5 protein expression was found in $GCN5^{KO}$ HAP1 cell compared to WT cell in Figure 4.2. In addition, the abolishment of GCN5 and PCAF in HAP1 cells was confirmed due to the absence of signals.

This result verified the inactivation of *GCN5*, *PCAF* and both genes in HAP1 cell lines by *Horizon Discovery*. These cells were used to study the influence of GCN5 and PCAF on the cellular proliferation or DNA repair.

## 4.1.2. Characterization of histone acetylation level
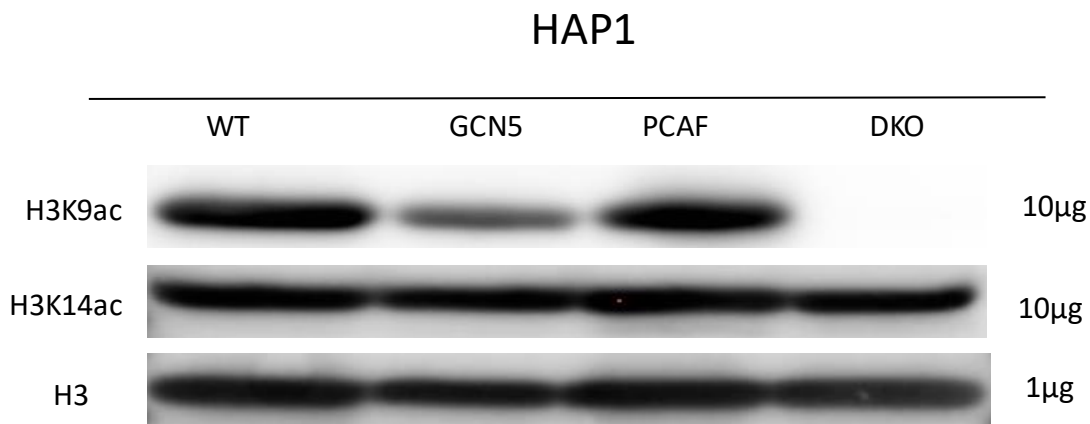
Figure 4.3. Western blot analysis of histone acetylation of acid extracts. Analysis with antibodies against acetyl-H3K9, acetyl-H3K14 and acetyl-H3. Amounts of protein is indicated.

Chromatin is the compacted structure consisting of H2A, H2B, H3 and H4. To allow DNA repair factors to access to the damaged sites, the chromatin needs to be opened and histone acetylation is one alternative to do that.

In addition, GCN5 and PCAF are capable of acetylating multiple lysine residues on histone H3 such as H3K9 and H3K14. By western blot analysis, I found out that deletion of *GCN5* in HAP1 cells affected slightly on the global level of histone acetylation H3 on lysine 9 while the abolishment of *PCAF* showed no effect compared to WT HAP1 cell. Additionally, $GCN5^{KO}PCAF^{KO}$ HAP1 showed lack of H3K9ac (Figure 4.3). Using the anti-H3K14ac antibody, I confirmed that the combined deletion of *GCN5* and *PCAF* had no effects on the global level of H3K14ac in HAP1 cells.

Taken together, these results confirmed that GCN5 and PCAF are redundant and specifically required for the acetylation of H3K9 in HAP1 cell lines.

4.1.3. Cellular proliferation
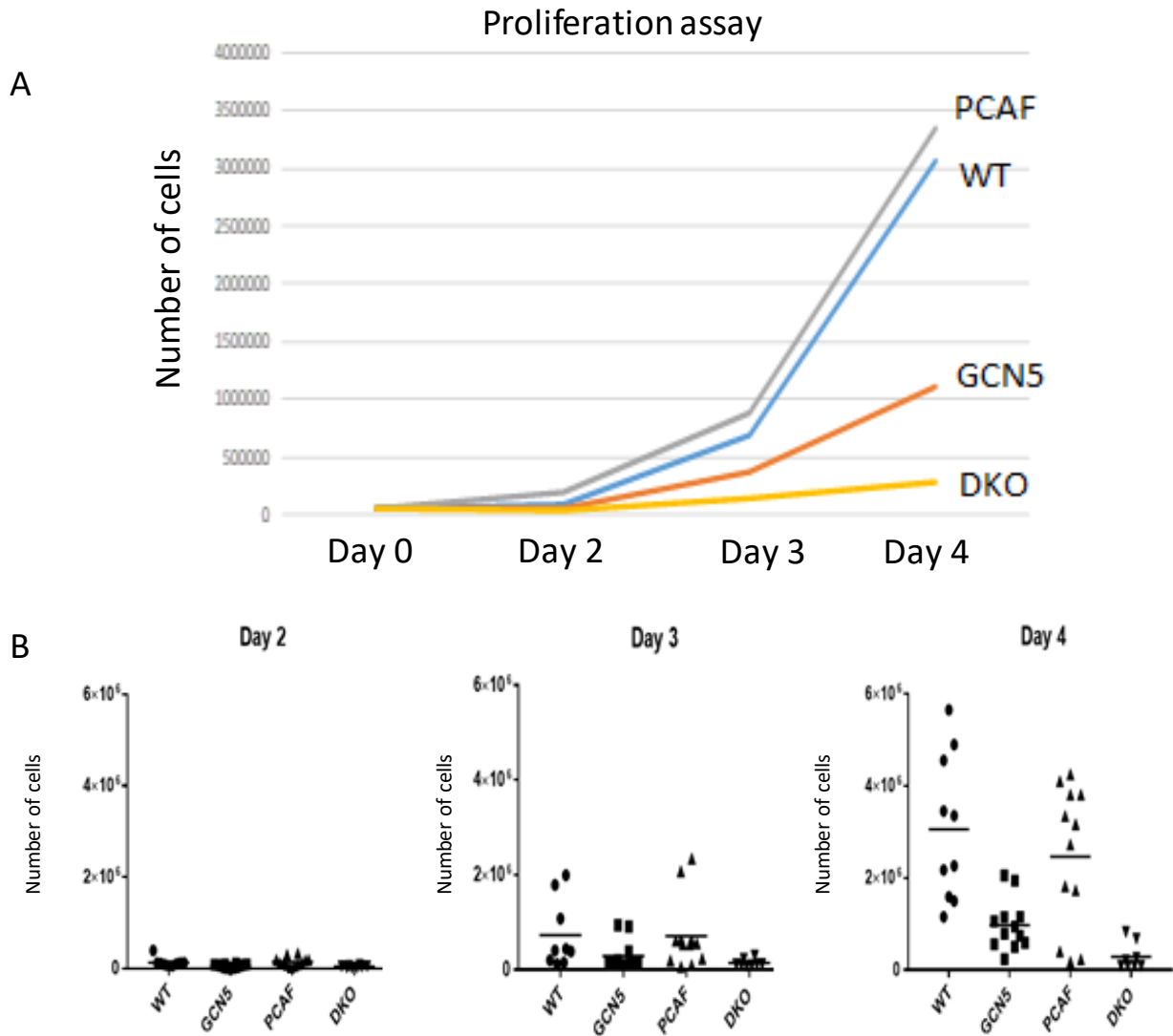
Figure 4.4. Proliferation of WT, *GCN5^{KO}*, *PCAF^{KO}* and *GCN5^{KO}PCAF^{KO}* HAP1 cell lines. A) Cells of indicated genotype cell lines were counted at 48, 72 and 96 hours after plating. The graph showed representatives of ten experiments. B) Statistical analysis was performed by using one-way ANOVA, GraphPad Prism 7.03

Proliferation assays were carried out to examine effects of single deletions of *GCN5* and *PCAF* and double deletion of *GCN5* and *PCAF* on cell growth. There was no much difference in growth rates between WT and *PCAF^{KO}* HAP1 cells, indicating that PCAF might play minor role during the proliferation. In contrast, deletion of *GCN5* caused 3-fold decrease in growth rate compared to those of WT and *PCAF^{KO}* HAP1 cell lines. This result was especially clear at day 4 when WT and

PCAF-deficient cells grew faster. Combined inactivation of *GCN5* and *PCAF* vastly decreased the proliferation rate of HAP1 cells (Figure 4.4). To conclude, GCN5 and PCAF have the redundant function on cellular proliferation. This result is consistent with the previous observation that $Gcn5^{-/-}/Pcaf^{-/-}$ mice died at an earlier embryonic stage than $Gcn5^{-/-}$ mice (Xu *et al,* 2000; Yamauchi *et al,* 2000).

Multiple comparisons between 4 groups during 3 days with one-way ANOVA, GraphPad Prizm 7.03:

Day 2: **WT** vs GCN5, p=0.1548 (n.s); **WT** vs PCAF, p=0.9341(no significance, n.s); **WT** vs DKO, p=0.0737(n.s); GCN5 vs PCAF, p=0.0258(*); GCN5 vs DKO, p=0.9323 (n.s); PCAF vs DKO, p=0.0126(*).

Day 3: **WT** vs GCN5, p=0.2794(n.s); **WT** vs PCAF, p=0.9998 (n.s); **WT** vs DKO, p=0.1417(n.s); GCN5 vs PCAF, p=0.2551(n.s); GCN5 vs DKO, p=0.9365(n.s); PCAF vs DKO, p=0.1256 (n.s).

Day4: **WT** vs GCN5, p=0.0010(**); **WT** vs PCAF, p=0.6450 (n.s); **WT** vs DKO, p<0.0001(****); **GCN5** vs PCAF, p=0.0176(*), **GCN5** vs DKO, p=0.5843 (n.s); PCAF vs DKO, p=0.0013(**).

In this statistical analysis, p-value or probability value was used as measure. This was used to evaluate how well the data support that the null hypothesis was true. Null hypothesis states that there is no significant different between specified population. Hence, low p-value could be used to reject the null hypothesis. As presented above, in day 4, the p-values between WT and DKO, $PCAF^{KO}$ and DKO, WT and $GCN5^{KO}$ were 0.0001%, 0,0013% and 0,0010%, respectively. This indicated that the difference in growth rate between these indicated genotype cell lines were significant. On day 2 and day 3, the difference was not clear.

Taken together, this result showed that the double deletion of *GCN5* and *PCAF* and single knockout of *GCN5* exerted profound negative effects in the growth rates of HAP1 cells while deletion of *PCAF* in HAP1 cells did not have any visible consequences.

4.1.4. Cell cycle analysis

Slow proliferation of HAP1 cells lacking both GCN5 and PCAF could be explained by the cell cycle modulation. Specifically, cell cycle is regulated by the activities of cyclin-CDKs. In addition, histone acetylation correlates with gene activation (Kaimori *et al,* 2016). Deletions of *PCAF* and

GCN5 may inhibit the expression of genes that are responsible for regulating cell cycle and consequently, cell cycle distribution may be changed. It is consistent with the fact that deletion of *GCN5* caused the delayed in G1 to S phase progression (Kikuchi *et al*, 2005).

The cell cycle result from this assay was unable to answer the original doubt because HAP1 cells started to convert to diploid state. Specifically, Figure 4.5 showed that in *GCN5^{KO}* and *PCAF^{KO}* HAP1 cell lines, the number of G1-phase cells were nearly 450 while in WT HAP1 cell, the recorded number was 120. In *GCN5^{KO}PCAF^{KO}* HAP1 cell lines, nearly 300 cells were arrested in G1 phase. To conclude, some cells were converted to diploid indicated by subsequent peaks after G2 phase cell and some of them remain haploid. Thus, it was hard to compare and due to limited time, I cannot continue.
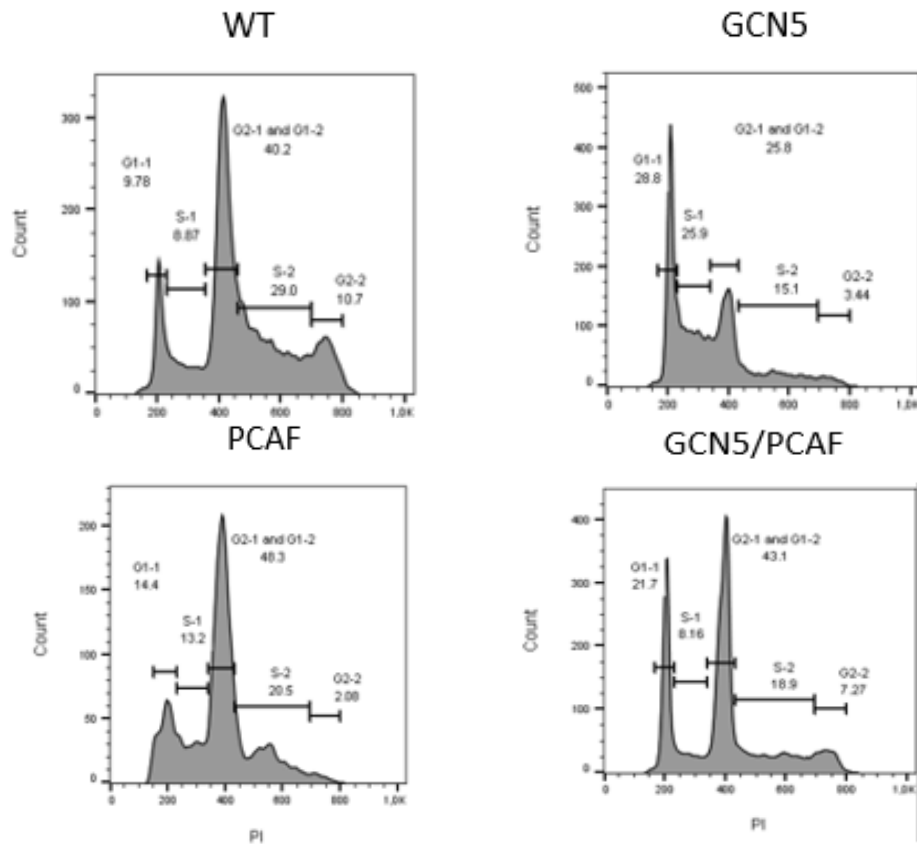

Figure 4.5. Cell cycle analysis of WT, *GCN5^{KO}*, *PCAF^{KO}* and *GCN5^{KO}PCAF^{KO}* HAP1 cell lines. Indicated genotype cell lines were cultured in the same conditions during 96 hours. G1-phase cell was demonstrated as the highest peak while G2-phase cell was shown as the second highest one. S-phase cell was depicted as region between G1 and G2-phase cells.

4.2. vAbl

4.2.1. Generation of *Pcaf⁻/⁻* vAbl cell lines

As mentioned earlier, vAbl is a suitable cellular model to study the V(D)J recombination. I employed CRISPR/Cas9-mediated gene editing to generate the vAbl pro-B cell line deficient for *Pcaf* by deleting this gene from the wild-type (WT) vAbl pro-B cells. In this experiment, single guided RNA (sgRNA) was used to achieve the knockout cell lines, western blot was performed to select the pool that expressed the lowest protein level signal indicating that there was a high probability to achieve the knockout cell lines. As shown in Figure 4.6, cellular pool 2A was selected to be sub-cloned.
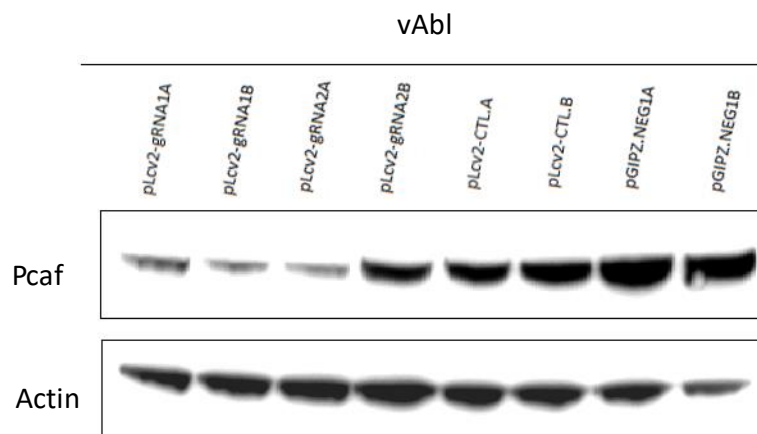
Figure 4.6. Western blot of vAbl cellular pools. pLcv2-gRNA (1A,1B,2A,2B) pools contain modified cell lines, pLcv2-CTL (A, B) was the plasmid which did not have the puromycine-resistant cassette and it was used as negative control during puromycine selection; pGIPZ.NEG (1A, 1AB) were used as positive controls for successful transfection as it contains GFP cassette. Equal amounts of cell extracts were run on SDS-PAGE prior to immunoblotting. The level of actin was also checked by monoclonal anti-actin antibody as internal control.

Then, there were nearly 50 clones to be selected for western blot experiment. Twenty eight of the total clones was deficient of *Pcaf*. This was confirmed by western blot. (Figure 4.7).

vAbl

	26	27	28	29	30	31	32	33	34	35	WT
Pcaf											
Actin											
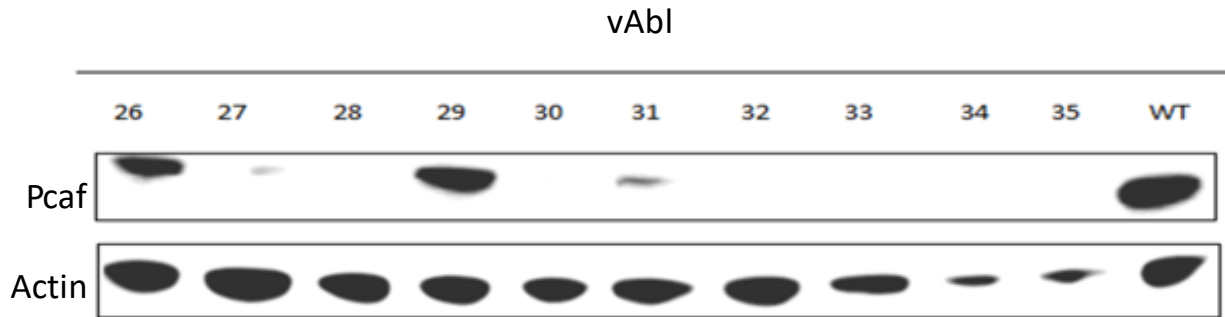
Figure 4.7. Determination of expression level of Pcaf protein in vAbl cells by western blot. The level of actin was also checked by monoclonal anti-actin antibody as internal control. Equal amounts of cell extracts were run on SDS-PAGE prior to immunoblotting.

4.2.2. V(D)J recombination assay
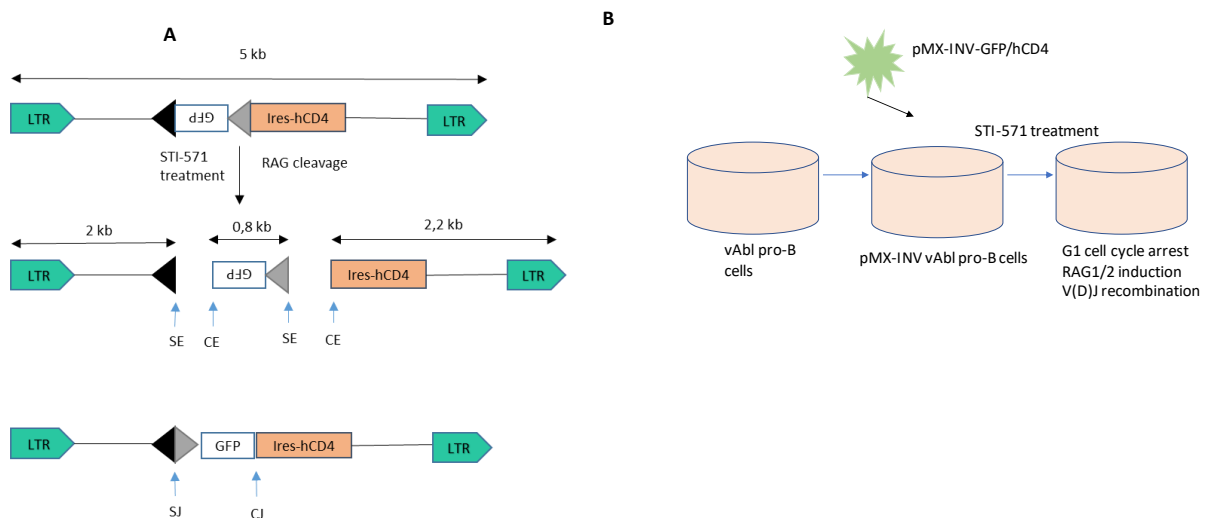
Figure 4.8. Procedure of V(D)J recombination assay in vAbl pro-B cells. A) Representation of structure of pMX-INV plasmid. The 12-recombination signal sequence (RSS-12), GFP cDNA, 23-recombinational signal sequence (RSS-23), IRES-human CD4 cDNA (IRES-hCD4), long-term terminal repeat (LTR), coding end (CE), signal end (SE), coding joint (CJ), signal joint (SJ) are indicated. B) The pMX-INV plasmid is introduced into the vAbl pro-B cells by retroviral transduction and integrated cells were enriched based on human CD4 (hCD4) expression. To perform V(D)J recombination assay, integrated cells were treated with 3μM tyrosine kinase inhibitor Imatinib STI-571 during 96 hours.

The acetyltransferase Gcn5 is involved in the DDR response and is functionally redundant with PCAF (both enzymes perform their functions on H3 at lysine 19) (Evangelia *et al,* 2017). Previous

studies showed that *Pcaf*-deficient mice were live-born while the deficiency of *Gcn5* lead to the embryonic lethality (Xu *et al,* 2010; Yamauchi *et al,* 2000). The *Gcn5^-/-^Pcaf^+/-^* mice even died earlier at the embryonic stage than *Gcn5^-/-^* mice. Our preliminary data showed that the *Gcn5^-/-^Pcaf^+/-^* double knockout mice, where *Gcn5* was inactivated conditionally in B cells only while *Pcaf* was inactivated in all organs, had smaller spleen compared to those of WT mice and single knockouts *Gcn5^-/-^* (conditionally inactivated in B cells only) and *Pcaf^+/-^* mice. In addition, the number of mature B cells in spleen was also low. In the blood of *Gcn5^-/-^Pcaf^+/-^* mice, the low number of B lymphocytes also were observed. Furthermore, the proportion of pro-B cells in bone marrow of WT, *Gcn5^-/-^, Pcaf^+/-^* and *Gcn5^-/-^Pcaf^+/-^* mice were 17%, 46%, 22% and 73%, respectively (Oksenych *et al,* unpublished data). From these records, it was hypothesized that Gcn5 and Pcaf may have the important role in early B cell development and the deficiencies of both enzymes may contribute to the arising of B lymphocytopenia.

Very low counts of mature B cells and the accumulation of immature pro-B cells can be caused by a defect in V(D)J recombination in *Gcn5^-/-^Pcaf^+/-^* mice. To determine the role of Gcn5 and Pcaf on efficiency of V(D)J recombination, I employed CRISPR/Cas9-mediated gene editing to generate vAbl pro-B cell lines deficient of *Gcn5* and *Pcaf*. Abolishment of these factors was confirmed by western blot. In addition, *Dna-Pkcs^-/-^Xlf^-/-^* vAbl cells were used as the negative controls because these genes were important during V(D)J recombination. Typically, DNA-PKcs is recruited to the DNA damaged sites to form the DNA repair complex with Ku70/80 heterodimer. Without DNA-PKcs, cells were vulnerable to radioactivity, possessed impaired DNA repair and prolonged the cell cycle arrest (Dong *et al*, 2018). In addition, together with XRCC4, XLF forms a structure to bring the DNA damaged ends for efficient ligation (Hummel *et al,* 2010; Wang *et al*, 2018). Additionally, DNA-PKcs and XLF have overlapping functions in NHEJ, thus the combined knockout of these genes abrogates joining of signal ends (SEs) within chromosomally intergrated V(D)J recombination substrates in vAbl pro-B cells (Oksenych *et al,* 2013). These negative control cell lines are available at our laboratory.

To analyze V(D)J recombination, chromosomally-integrated cassette was used. Specifically, I transduced WT, *Pcaf^+/-^* and *Dna-Pkcs^-/-^Xlf^-/-^* vAbl pro-B cells with the pMX-INV plasmid that could express GFP after successful inversional recombination. pMX-INV contains inverted fluorescent protein (GFP) cassette flanked by recombination signal sequences (Figure 7.8) that can

be cleaved and inverted back to the same orientation as the promoter (Lenden *et al,* 2017). Then, WT, *Pcaf^-/-^* and *Dna-Pkcs^-/-^Xlf^-/-^* vAbl pro-B cells were treated with the vAbl kinase inhibitor STI-571 (Imatinib) for 96 hours (Figure 7.9) that result in the G1 arrest (55,6% in WT, 54,1% in *Pcaf^-/-^* and 42,2% in *Dna-Pkcs^-/-^Xlf^-/-^*); the cell death of these cell lines were 36,6% in WT, 32,4% in *Pcaf^-/-^* and 36% in *Dna-Pkcs^-/-^Xlf^-/-^* (Figure 7.9).
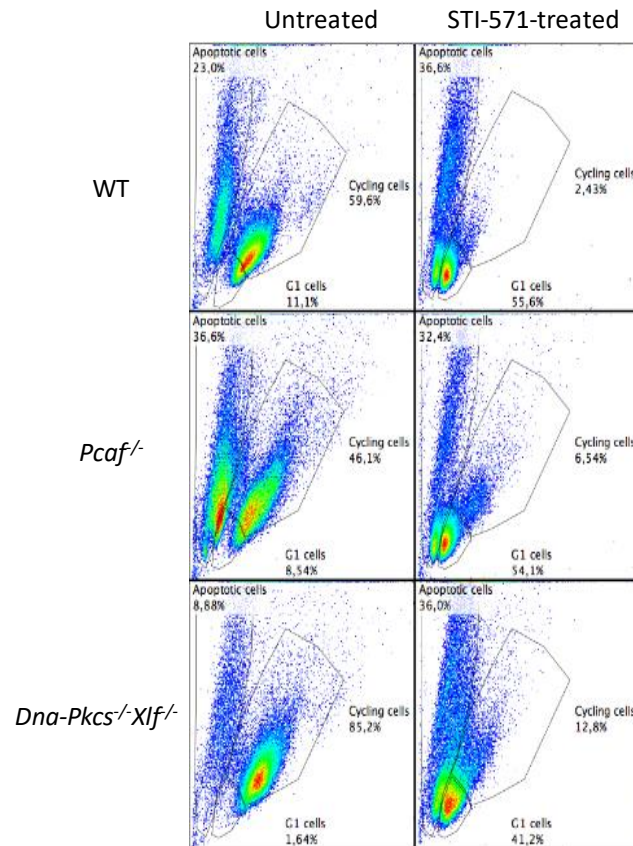

Figure 4.9. Representative examples of gating for WT, *Pcaf^-/-^* and *Dna-Pkcs^-/-^Xlf^-/-^* vAbl cells. STI-571 cells treated indicated: apoptotic, cycling and G1 arrested cells are shown.
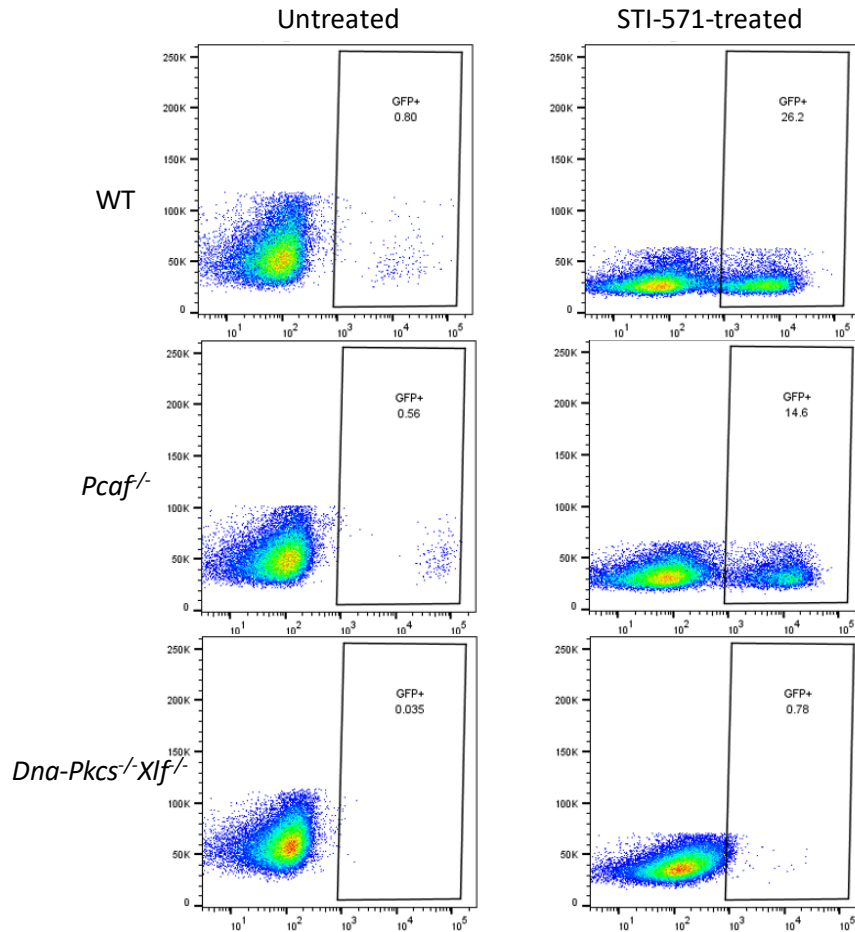
Figure 4.10. V(D)J recombination efficiencies in WT, *Pcaf^{-/-}* and *Dna-Pkcs^{-/-}Xlf^{-/-}* vAbl pro-B cells. These results were analyzed by FACS and presented as the percentages of GFP⁺ cells among the total hCD4⁺ cells. The proportions of GFP positive cells in STI-571-treated WT, *Pcaf^{-/-}* and *Dna-Pkcs^{-/-}Xlf^{-/-}* were 26.2%, 14.6% and 0.78%, respectively.

Arresting the cells at the G1 cell cycle phase triggers the expression of RAG1/2, which in turn initiates the V(D)J recombination (Arya and Bassing, 2017). By using this assay, integrated pMX-INV substrate was rearranged in WT and *Pcaf^{-/-}* cells with similar efficiency. Typically, 16% of WT cells recombined which were measured as proportion of GFP positive cells, while those of *Pcaf^{-/-}* and *Dna-Pkcs^{-/-}Xlf^{-/-}* were 10,5% and 0%, respectively (Figure 4.10). Average results of three independent experiments were shown in Figure 4.11. To conclude, chromosomal V(D)J recombination is robust in cells lacking Pcaf.
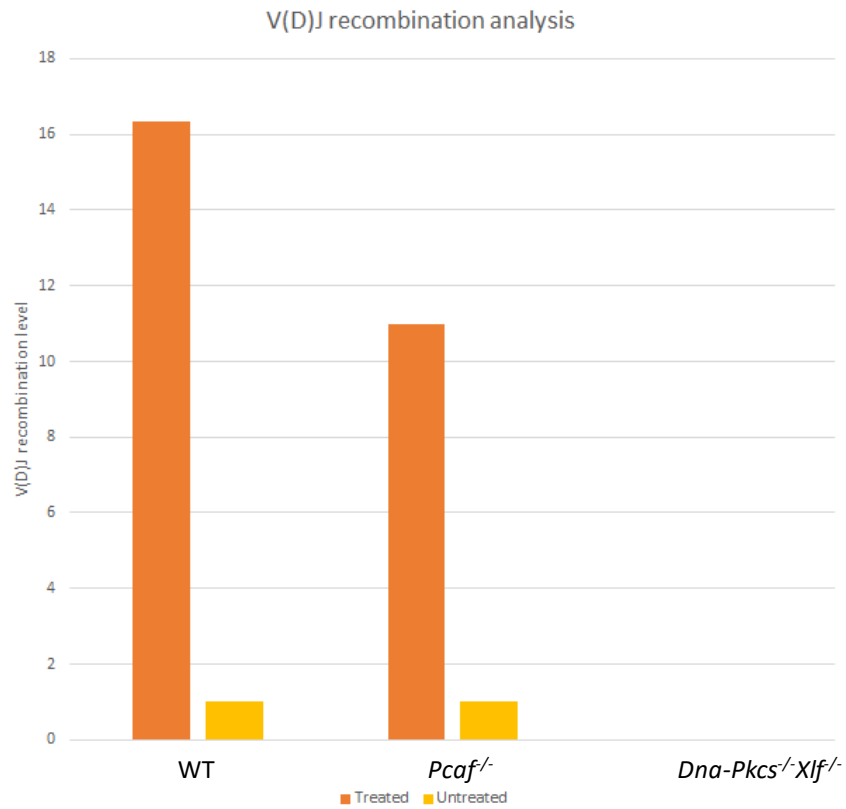
Figure 4.11. Graphical representation of V(D)J recombination efficiency. WT, *Pcaf*$^{-/-}$ and *Dna-Pkcs*$^{-/-}$*Xlf*$^{-/-}$ vAbl pro-B cells efficiency are shown. The results are the mean of three independent experiments

In this thesis, the generation of *Gcn5*$^{-/-}$ and *Gcn5*$^{-/-}$*Pcaf*$^{+/-}$ vAbl pro-B cell lines were not achieved. CRISPR/Cas9-editing strategy was time-consuming experiment and it took several months to inactivate the desired genes. In addition, the proportion of cells which inactivated gene of interest was low as evidence by western blot. Thus, experiments with the aim of inactivating *Gcn5* and together *Gcn5/Pcaf* were not carried out due to the limited time.

4.3. CH12F3

4.3.1. Generation of *Gcn5^{-/-}* and *Pcaf^{-/-}* CH12F3 cell lines

As mentioned earlier, CH12F3 was proven to be a suitable candidate to study the Class Switch Recombination. To study the role of Gcn5 and Pcaf during CSR, I inactivated these acetyltransferases by CRISPR/Cas9 gene editing strategy. Specifically, two single-guide RNAs that targeted either *Gcn5* or *Pcaf*, were transduced into wild-type CH12F3 cells. After treatment with puromycine for one week, the cellular pool which had the lowest protein expression level was sub-cloned. Lack of corresponding protein was verified by western blot analysis. As Figure 4.12 showed, the cellular pool 1A was used to sub-clone.
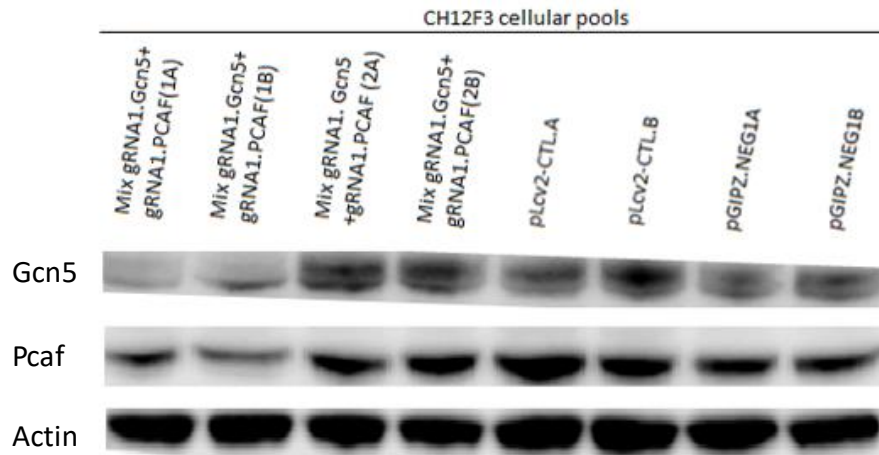
Figure 4.12. Western blot analysis of CH12F3 cellular pools. Mix pLcv2-gRNAs (1A,1B,2A,2B) were used to inactivate *Gcn5* and *Pcaf* in WT CH12F3 cells, pLcv2-CTL (A, B) was the plasmid which did not have the puromycine-resistant cassette, it was used as negative control during puromycine selection; pGIPZ.NEG (1A, 1AB) were used as positive controls for successful transfection because it encodes *GFP*. Equal amounts of cell extracts were run on SDS-PAGE prior to immunoblotting. The level of actin was also checked by monoclonal anti-actin antibody as internal control.

Then, the clones were also verified by western blot analysis to screen for the targeted gene-deficient cells. *Gcn5^{-/-}* (clone 3) CH12F3 cell line and *Pcaf^{-/-}*(clone 34) CH12F3 were used for experiments (Figure 4.13).

Figure 4.13. Determination of expression level of Gcn5 and Pcaf proteins in CH12F3. The level of actin was also checked by using monoclonal-actin antibody as internal control. Equal amounts of cell extracts were run on SDS-PAGE prior to immunoblotting.

The generation of double knockout $Gcn5^{-/-}Pcaf^{-/-}$ CH12F3 cell lines was not done due to time limit.

4.3.2. Characterization of histone acetylation
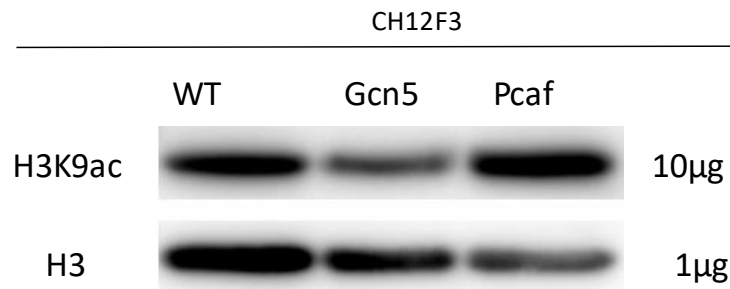
Figure 4.14. Western blot of histone acetylation of acid extracts WT, $Gcn5^{-/-}$ and $Pcaf^{-/-}$ CH12F3 cell lines. Analysis with antibodies against acetyl-H3K9, and acetyl-H3.

I also performed the western blot analysis for global histone level in WT, $Gcn5^{-/-}$ and $Pcaf^{-/-}$ CH12F3 cell lines. I verified the effect of deletions of these genes on histone acetylation. Deletion of *Gcn5* resulted in reduced global level of H3K9ac while inactivation of *Pcaf* in CH12F3 cell lines did not have any effects on H3K9 acetylations (Figure 4.14). In the $Gcn5^{-/-}Pcaf^{-/-}$ CH12F3 cell line, the global level of H3K9ac might be abolished compared to WT and Pcaf cell lines. It was consistent with the studies showing that the common substrate of *Gcn5* and *Pcaf* was H3K9 (Church *et al,* 2017). To conclude, Gcn5 and Pcaf have the overlapping functions.

4.3.3. Proliferation assay
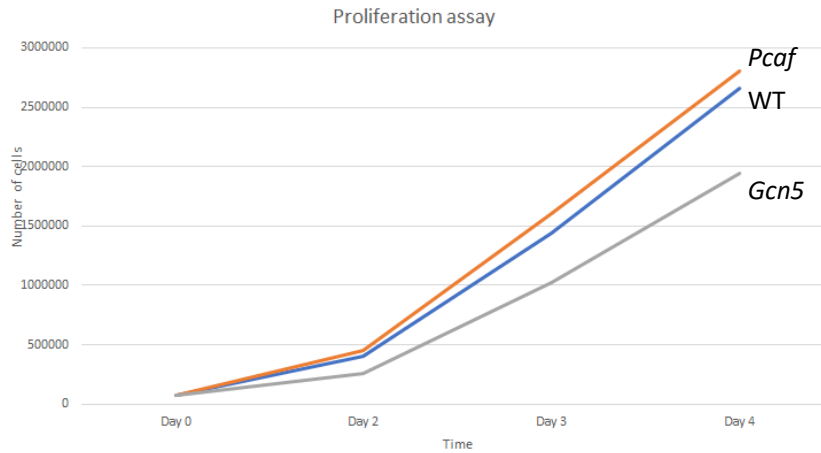
Figure 4.15. Proliferation assay of WT, *Gcn5*$^{-/-}$ and *Pcaf*$^{-/-}$ CH12F3 cell lines. Proliferation of indicated genotypes in CH12F3 cell was measured at 48, 72 and 96 hours. The graph showed the representative of five independent experiments.

Before trying to understand the role of Gcn5 and Pcaf in CSR, proliferation assay was carried out. B cell differentiation and isotype switching correlate with number of cell division (Hodgkin *et al,* 1996). Two complete rounds of cell division are required for IgG and IgA CSR. (Deenick EK *et al,* 1999). Lastly, I also wanted to check whether the deletion of *Gcn5* and *Pcaf* in CH12F3 cell lines show similar effects to those of HAP1 cells.

As presented in Figure 4.15, there was no much difference in growth rate between *Pcaf*$^{-/-}$ CH12F3 and wild type cells. This is consistent with finding in HAP1 cell lines. In contrast, while deletion of *Gcn5* showed 2-fold decrease in growth rates in HAP1 cells, there was only a slight difference between the WT and *Gcn5*$^{-/-}$ CH12F3 cells. In conclusion, Gcn5 regulates proliferation of CH12F3 cells while Pcaf is dispensable for cell proliferation in this model system.
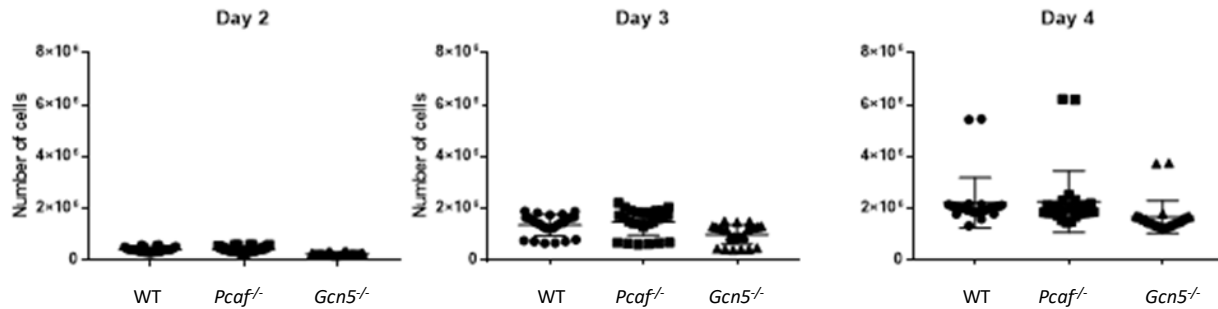
Figure 4.16. Statistical analysis performed by GraphPad Prism 7.0. The result of day 2, day 3 and day 4 were analyzed, each dot represents for one result.

Multiple comparisons between 3 groups during 3 days with one-way ANOVA, GraphPad Prizm 7.03.

Day 2: **WT** vs *Gcn5*, p=0.5548 (no significant, n.s); **WT** vs *Pcaf*, p=0.9341 (n.s); *Gcn5* vs *Pcaf*, p=0.7585 (n.s)

Day 3: **WT** vs *Gcn5*, p=0.3759(n.s); **WT** vs *Pcaf*, p=0.8192 (n.s); *Gcn5* vs *Pcaf*, p=0.3759(n.s).

Day4: **WT** vs *Gcn5*, p=0.0010(**); **WT** vs *Pcaf*, p=0.6450 (n.s); *Gcn5* vs *Pcaf*, p=0.0010 (**)

In the statistical analysis, p-value again was used as a measure to determine if there was a difference between tested cell lines. As presented in Figure 4.16, in each cell line, the result arising from counting experiment was close. On day 2 and day 3, the difference between samples was not significant. On day 4, the results from WT and *Pcaf*^-/- CH12F3 cell lines did not have much difference while both of them showed the higher rate of proliferation compared to that of *Gcn5*^-/- CH12F3 cell lines.

Taken together, although the proliferation assays were carried out in both human and mouse cell lines, the results were almost similar between the species. Gcn5 induced a small defect on the growth rate while Pcaf did not have any effect.

4.3.4. Class Switch Recombination assay
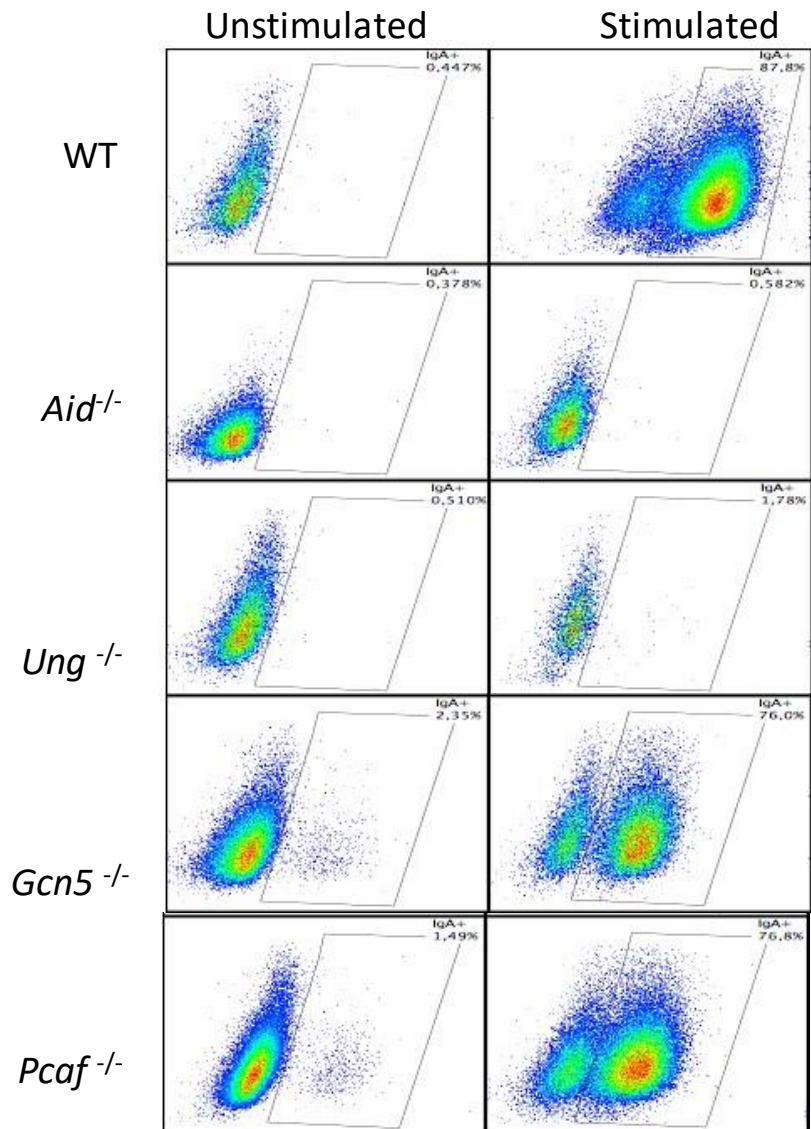
Figure 4.17. Class switch recombination assay in WT, *Aid⁻ᐟ⁻*, *Ung ⁻ᐟ⁻*, *Gcn5 ⁻ᐟ⁻* and *Pcaf ⁻ᐟ⁻* CH12F3 cell lines. In the left panel, switching level from IgM to IgA of unstimulated cell lines were shown. In the right panel, the CSR efficiency of these indicated genotypes were analyzed by FACS and presented as percentages after being stimulated during 96h.

Following V(D)J recombination, AID cytosine deaminase initiates another set of DNA breaks in mature B cells to ensure the lymphocyte specialization during class switch recombination (CSR). CSR-induced DNA double breaks are repaired by the NHEJ as described in Introduction part. However, these breaks also activate the DDR. By date, *Gcn5* and *Pcaf*, have no documented effect

on the CSR. To determine the impact of Gcn5 and Pcaf on CSR to IgA, I inactivated *Gcn5* and *Pcaf* genes in CH12F3 cell lines, and perform the CSR experiments.

First, I employed the CRISPR/Cas9 editing strategy to inactivate *Gcn5* and *Pcaf* in CH12F3 to generate the *Gcn5*^{-/-} and *Pcaf*^{-/-} single knockout CH12F3 cell lines. The lack of protein was confirmed by western blot analysis (Figure 4.13). Additionally, *Aid*^{-/-} and *Ung*^{-/-} CH12F3 cell lines were used as negative controls. Both AID and UNG are involved in the initiation of CSR. The function of AID has been mentioned in Introduction part at section 1.3.2. UNG removes the dU enzymaticallt by BER pathway and CSR is reduced 95% in B cells lacking UNG, either derived from UNG deficient mice or from patients that have deleterious mutation in UNG (Nielsen *et al,* 2000; Schrader *et al,* 2005). *Aid*^{-/-} and *Ung*^{-/-} CH12F3 cell lines are available in our laboratory and generated by Bodil Kavli group recently (Dewan *et al*, 2018). Cells of indicated genotypes were stimulated with Il-4, CD40L and TGF-B to activate the switching from IgM to IgA and incubated for 96 hours. Flow cytometry showed that nearly 90% of stimulated WT cells switched to IgA while stimulated only 76% of *Gcn5*^{-/-} and 77% of *Pcaf* were IgA positive. *Aid*^{-/-} and *Ung*^{-/-} CH12F3 showed almost 0% in switching, as expected (Nielsen *et al,* 2000; Okazaki, Honjo *et al*, 2002; Dewan *et al*, 2018). Control unstimulated cells did not switch to IgA (switching control, Figure 4.17). This result was surprising because as Figure 4.15 and Figure 4.16 presented, there was a difference in proliferation in *Gcn5*^{-/-} and *Pcaf*^{-/-} CH12F3 cells and earlier data suggested that inactivation of *Gcn5* might have more stronger effect on CSR than inactivation of *Pcaf*. To conclude, based on my observations, deletions of either *Gcn5* or *Pcaf* resulted in reduced CSR to IgA.

5. DISCUSSION

This work was initiated to decipher how GCN5 and PCAF regulate some major events during the development of B lymphocytes, particularly, in proliferation, V(D)J recombination and CSR. Cell lines-based experiments were designed to characterize the functional properties of these acetyltransferases. GCN5 and PCAF acetyltransferases are functionally redundant, e.g. they both acetylate H3K9 (Lee *et al,* 2010). One might expect that GCN5 and PCAF would have similar effect on the cellular processes. Based on my observations, that expectation is confirmed, both these proteins are important during the B lymphocyte development.

Two different cell types from two species, human HAP1 lines $GCN5^{KO}$, $PCAF^{KO}$, $GCN5^{KO}PCAF^{KO}$ and murine $Gcn5^{-/-}$ and $Pcaf^{-/-}$ CH12F3 cells were used to perform the proliferation assay. Western blot analysis confirmed the deficiency of the acetyltransferases in corresponding cell lines. The experiments were repeated at least twice to confirm the results. Additionally, the effects of *Gcn5* and *Pcaf* deletion on the acetylation of histone H3K9 and H3K14ac were also analyzed. In agreement with my results, human and yeast *GCN5* were indicated to acetylate H3K9 among the four core histones (Evangelia *et al,* 2017). In addition, as shown in Figure 7.3, $GCN5^{KO}PCAF^{KO}$ HAP1 did not reduce the global level of H3K14ac, indicating that other HATs can compensate functions of GCN5 and PCAF. In another context, it is expected that GCN5 and PCAF should have certain roles during the proliferation (Kikuchi *et al,* 2016). In this study, GCN5 was probably involved in the controlling of growth rate but PCAF seemed to be dispensable for proliferation (Figure 4.4 and Figure 4.15). My results are in line with the new study showing that deletion of *Gcn5* inhibits short-term and long-term proliferation, while knockout of *Pcaf* showed minor effects on proliferation of urothelial carcinoma cells (Evangelia *et al*, 2017). The delayed growth rate of $GCN5^{KO}$ HAP1 and $Gcn5^{-/-}$ CH12F3 might be explained by the alterations in the cell cycle distribution. Another study also showed that *Gcn5*-deficient mouse embryonic fibroblasts (MEFs) grew slower due to the delayed progression from G1 to S phase, while this phenomenon was not observed in the case of *Pcaf* knockout (Kikuchi *et al,* 2005). $GCN5^{KO}PCAF^{KO}$ HAP1 cells grew slower compared to that of $GCN5^{KO}$ HAP1 cells. It was consistent with the observation made using mouse model as $Gcn5^{-/-}Pcaf^{-/-}$ mice died earlier at the embryonic stage than $Gcn5^{-/-}$ mice (Xu *et al,* 2000; Yamauchi et al, 2000). To elucidate more about

the role of GCN5 and PCAF during B cell development in HAP1 cell lines, V(D)J recombination and CSR assays need to perform.

WT, *Pcaf^-/-* and *Dna-Pkcs^-/-/Xlf^-/-* vAbl cells carrying the *Bcl2* to reduce apoptosis after treating with STI-571, were used to study the V(D)J recombination. These pro-B cells were transduced with pMX-INV-containing retroviral vectors. The negative controls showed no rearrangements, this was consistent with the role of DNA-PKcs in V(D)J recombination (Gao Y *et al,* 1998). WT vAbl cells switch to the level of 16% which was lower than observed by others (Lenden *et al,* 2017). The difference in rearrangement level between mine and other studies might be explained by experimental setup or by using different cell lines despite the same genetic background. V(D)J recombination reporter assays revealed that Pcaf is dispensable for V(D)J recombination. This result was confirmed by comparing the recombination levels of cells that have deficiencies in *Pcaf* to those of WT and *Dna-Pkcs^-/-Xlf^-/-* vAbl cells. This finding was supported by the analysis of animal models where number of mature B cells in spleen and blood was nearly normal in the absence of Pcaf. To elucidate the role of Gcn5 in V(D)J recombination and whether Gcn5 and Pcaf are overlap functions during V(D)J recombination, generations of *Gcn5^-/-* and *Gcn5^-/-Pcaf^-/-* vAbl cell lines and functional analysis needs to be performed in the future. To conclude, CRISPR/Cas9-edited vAbl pro-B cells provide the physiological surrogate *ex vivo* system to study the function of targeted genes during V(D)J recombination. vAbl pro-B cells were also confirmed as a valuable experiment system to study the V(D)J recombination including aspects of DNA repair during the last decade (Bredemeyer *et al,* 2006; Lenden *et al,* 2017).

In another context, I have studied specific roles of Gcn5 and Pcaf in class switch recombination. It is a known fact that cell cycle divisions associates with the CSR (Hodgkin *et al,* 1996). As mentioned, the deletion of *Pcaf* does not have any influence on the growth rate of cells but deletion of *Gcn5* affected proliferation (Figure 7.3 and 7.13). Hence, *Gcn5*-deficient CH12F3 cells might have lower level switching from IgM to IgA compared to that of *Pcaf* and WT. In this regard, the results seem to be difficult to reconcile with the achieved results in proliferation assay by showing the non-significant difference between *Gcn5* and *Pcaf* in CSR. However, by comparing the recombination levels of single knockout *Gcn5^-/-* and *Pcaf^-/-* CH12F3 cells to those of WT and *Aid^-/-* and *Ung^-/-* CH12F3 cell lines (Figure 7.16), my results support the finding that Gcn5 and Pcaf might exert their functions in CSR. This was consistent with another study showing that deletions

of both *Gcn5* and *Pcaf* could abort the CSR, in spite of different reasons (Li *et al,* 2014). Although the role of Gcn5 and Pcaf was studied in this thesis, whether they have overlapping function was not investigated. To answer question on genetic interaction between *Gcn5* and *Pcaf*, generation of *Gcn5$^{-/-}$Pcaf$^{-/-}$* CH12F3 cells and functional CSR with those is required in the future. To conclude, either deletion of *Gcn5* or *Pcaf* possibly affected to the CSR level in CH12F3 cell lines. In addition, CRISPR/Cas9- edited CH12F3 cells was confirm again as the invaluable experiment set to study the role of specific genes in class switch recombination (Nakamura *et al*, 1996; Kim *et al*, 2016).

This work gave the general picture of the specific roles of GCN5 and PCAF acetyltransferases in B lymphocyte development. However, in this thesis, the exact mechanisms at which GCN5 and PCAF affect the V(D)J recombination and CSR are not clarified. In CSR, there are two mechanisms that play important roles. First, germline transcription (GLT) provides the substrate for AID to initiate CSR. Second, BER and NHEJ DNA repair pathways during recombination are necessary to both initiate and repair DSBs. Thus, impaired CSR may be explained by defects in GLT or DNA repair (Bahjat and Guikema, 2017). To study GLT, isolation of RNA and quantitative PCR (qPCR) can be applied to study the transcription efficiency at corresponding loci of immunoglobulin genes. If deletions of *Gcn5* and *Pcaf* do not have any influences on GTL, DNA repair efficiency can be studied. In another context, to study DNA repair, the cells are treated with etoposide or zeocin to induce DSBs and cells are counted one week post treatment. Another alternative is telomeric fluorescence *in situ* hybridization (T-FISH). Specifically, metaphase spreads are prepared and spontaneous chromosomal aberrations are counted by T-FISH assay (Hultdin *et al*, 1998). If the number of cell colonies in *GCN5/PCAF* double knockout cells treated with DSBs inducing chemicals is lower than that in WT cell and if frequency of chromosome breaks is higher in double knockout cells when compared to WT and single knockout controls, it may indicate that the combined inactivation of *GCN5* and *PCAF* limits DNA repair efficiency in B cells.

6. CONCLUSIONS

In this thesis, three different cell lines from two species human HAP1 and murine vAbl and CH12F3 were used to study the role of GCN5 and PCAF during the development of B lymphocytes and in general cell biology.

I found that combined inactivation of *GCN5* and *PCAF* in human HAP1 cells leads to lack of H3K9 acetylation and to reduced proliferation, when compared to WT or single knockout controls.

I generated murine vAbl cells lacking of *Pcaf* using CRISPR/Cas9 gene editing approach. In my experiments, Pcaf was dispensable for V(D)J recombination.

I generated knockout CH12F3 murine B cell lines lacking either Gcn5 and Pcaf. I demonstrated that level of CSR to IgA is reduced when either *Gcn5* and *Pcaf* is knocked out.

Overall, GCN5 and PCAF play the critical role during B lymphocyte development.

A

7. REFERENCES

1.Craxton A, Somers J, Munnur D, Jukes-Jones R, Cain K, Malewicz M, *XLS (c9orf142) is a new component of mammalian DNA double-stranded break repair.* Cell Death and Differentiation, 2015 Jun;22(6):890-7.

2. Abelson HT, Rabstein LS, *Lymphosarcoma: virus-induced thymic-independent disease in mice.* Cancer Res, 1970 Aug;30(8):2213-22.

3. Lukaszewicz A, Lange J, Keeney S, Jasin M, *Control of meiotic double-strand-break formation by ATM: local and global views.* Cell Cycle, 2018, Jul 2.

4. Kim A, Han L, Santiago GE, Verdun RE, Yu K,.Class-Switch Recombination in the Absence of the IgH 3' Regulatory Region. The Journal of Immunology, 2016 Oct 1;197(7):2930-5.

5. Dewan A, Xing M, Lundbæk MB, Gago-Fuentes R, Beck C, Aas PA, Liabakk NB, Sæterstad S, Chau KTP, Kavli BM, Oksenych V, *Robust DNA repair in PAXX-deficient mammalian cells.* FEBS Open Bio, 2018 Feb 7;8(3):442-448.

6. Davis AJ, Chen DJ, *DNA double strand break repair via non-homologous end-joining.* Transl Cancer Res, 2013 Jun;2(3):130-143.

7. Tubbs A, Nussenzweig A, *Endogenous DNA Damage as a Source of Genomic Instability in Cancer.* Cell, 2017 Feb 9;168(4):644-656.

8. Paul A, Wang B, *RNF8- and Ube2S-Dependent Ubiquitin Lysine 11-Linkage Modification in Response to DNA Damage.* Mol Cell, 2017 May 18;66(4):458-472.

9. Sibanda BL, Chirgadze DY, Ascher DB, Blundell TL, *DNA-PKcs structure suggests an allosteric mechanism modulating DNA double-strand break repair*, Science, 2017 Feb 3;355(6324):520-524.

10. Bredemeyer AL, Sharma GG, Huang CY, Helmink BA, Walker LM, Khor KC, Nuskey B, Sullivan KE, Pandita TK, Bassing CH, Sleckman BP, *ATM stabilizes DNA double-strand-break complexes during V(D)J recombination*. Nature, 2006 Jul 27;442(7101):466-70.

11. Chakraborty A, Tapryal N, et al, *Classical non-homologous end-joining pathway utilizes nascent RNA for error-free double-strand break repair of transcribed genes*. Nature Communication, 2016 Oct 5;7:13049.

12. Nemazee D, *Receptor editing in lymphocyte development and central tolerance.* Nature Reviews Immunology, 2006 Oct;6(10):728-40.

13. Dedeoglu F, Horwitz B, Chaudhuri J, Alt FW, Geha RS, *Induction of activation-induced cytidine deaminase gene expression by IL-4 and CD40 ligation is dependent on STAT6 and NFkappaB*. Int Immunol, 2004 Mar;16(3):395-404.

14. Deenick EK, Hasbold J, Hodgkin PD, *Switching to IgG3, IgG2b, and IgA is division linked and independent, revealing a stochastic framework for describing differentiation*. J Immunol, 1999 Nov 1;163(9):4707-14.

15. Hamilton DF, Ghert M, Simpson AH, *Interpreting regression models in clinical outcome studies.* Bone Joint Res, 2015 Sep;4(9):152-3.

16. Cortizas EM, Zahn A, Hajjar ME, Patenaude AM, Di Noia JM, Verdun RE, *Alternative end-joining and classical nonhomologous end-joining pathways repair different types of double-strand breaks during class-switch recombination* The Journal of Immunology, 2013 Dec 1;191(11):5751-63.

17. Koutsogiannouli EA, Wagner N, Hader C, Pinkerneil M, Hoffmann MJ, Schulz WA, *Differential Effects of Histone Acetyltransferase GCN5 or PCAF Knockdown on Urothelial Carcinoma Cells*. International Journal of Molecular Sciences, 2017 Jul 5;18(7). pii: E1449.

18. Yin FF, Bailey S, Innis CA, Ciubotaru M, Kamtekar S, Steitz TA, Schatz DG, *Structure of the RAG1 nonamer binding domain with DNA reveals a dimer that mediates DNA synapsis*. Nature Structure and Molecular Biology, 2009 May;16(5):499-508.

19. Gao Y, Chaudhuri J, Zhu C, Davidson L, Weaver DT, Alt FW, *A targeted DNA-PKcs-null mutation reveals DNA-PK-independent functions for KU in V(D)J recombination,* Immunity, 1998 Sep;9(3):367-76.

20. Coster G, Goldberg M, *The cellular response to DNA damage: a focus on MDC1 and its interacting proteins,* Nucleus,2010 Mar-Apr;1(2):166-78.

21. Li G, White CA, Lam T, Pone EJ, Tran DC, Hayama KL, Zan H, Xu Z, Casali P,

Combinatorial H3K9acS10ph histone modification in IgH locus S regions targets 14-3-3 adaptors and AID to specify antibody class-switch DNA recombination. Cell Reports, 2013 Nov 14;5(3):702-714.

22. Sáez GT, *DNA Damage and Repair in Degenerative Diseases 2016*, International Journal of Molecular Sciences, 2017 Jan 16;18(1). pii: E166.

23. Lee HS, Park JH, Kim SJ, Kwon SJ, Kwon J, *A cooperative activation loop among SWI/SNF, gamma-H2AX and H3 acetylation for DNA double-strand break repair.* EMBO J, 2010 Apr 21;29(8):1434-45.

24. Kikuchi H, Kuribayashi F, Mimuro H, Ohmi S I, *GCN5-deficiency remarkably enhances the sensitivity of B cells in response to 4-nitroquinoline 1-oxide*, Fundamental Toxicological Sciences, 2016; 3 (3):137-142.

25. Nilsen H, Steinsbekk KS, Otterlei M, Slupphaug G, Aas PA, Krokan HE, *Analysis of uracil-DNA glycosylases from the murine Ung gene reveals differential expression in tissues and in embryonic development and a subcellular sorting pattern that differs from the human homologues.* Nucleic Acids Res, 2000 Jun 15;28(12):2277-85.

26. Hodgkin PD, Lee JH, Lyons AB, *B cell differentiation and isotype switching is related to division cycle number.* J Exp Med, 1996 Jul 1;184(1):277-81.

27. Mu H, Geacintov NE, Min JH, Zhang Y, Broyde S, *Nucleotide Excision Repair Lesion-Recognition Protein Rad4 Captures a Pre-Flipped Partner Base in a Benzo[a]pyrene-Derived DNA Lesion: How Structure Impacts the Binding Pathway.* Chem Res Toxicol, 2017 Jun 19;30(6):1344-1354.

28. Chang HH, Watanabe G, Gerodimos CA, Ochi T, Blundell TL, Jackson SP, Lieber MR, *Different DNA End Configurations Dictate Which NHEJ Components Are Most Important for Joining Efficiency.* Journal of Biological Chemistry, 2016 Nov 18;291(47):24377-24389.

29. Chang HH, Lieber MR.*Structure-Specific nuclease activities of Artemis and the Artemis: DNA-PKcs complex.* Nucleic Acids Res, 2016 Jun 20;44(11):4991-7.

30. Okazaki IM, Kinoshita K, Muramatsu M, Yoshikawa K, Honjo T. *The AID enzyme induces class switch recombination in fibroblasts.* Nature, 2002 Mar 21;416(6878):340-5.

31. Imseng S, Aylett CH, Maier T, *Architecture and activation of phosphatidylinositol 3-kinase related kinases.* Curr Opin Struct Biol, 2018 Apr;49:177-189.

32. Watson JD, Crick FH, *A structure for deoxyribose nucleic acid. 1953*. Nature, 2003 Jan 23;421(6921):397-8.

33. Rush JS, Liu M, Odegard VH, Unniraman S, Schatz DG, *Expression of activation-induced cytidine deaminase is regulated by cell division, providing a mechanistic basis for division-linked class switch recombination.* PNAS, 2005 Sep 13;102(37):13242-7.

34. Sun J, Shi L, Kinomura A, Fukuto A, Horikoshi Y, Oma Y, Harata M, Ikura M, Ikura T, Kanaar R, Tashiro S, *Distinct roles of ATM and ATR in the regulation of ARP8 phosphorylation to prevent chromosome translocations.* Elife, 2018 May 8;7. pii: e32222.

35. Dong J, Ren Y, Zhang T, Wang Z, Ling CC, Li GC, He F, Wang C, Wen B, *Inactivation of DNA-PK by knockdown DNA-PKcs or NU7441 impairs non-homologous end-joining of radiation-induced double strand break repair.* Oncology Report, 2018 Mar;39(3):912-920.

36. Jiang J, Lu J, Lu D, Liang Z, et al, *Investigation of the acetylation mechanism by GCN5 histone acetyltransferase.* PLoS One, 2012;7(5): e36660.

37. Kaimori JY, Maehara K, Hayashi-Takanaka Y, Harada A, Fukuda M, Yamamoto S, Ichimaru N, Umehara T, Yokoyama S, Matsuda R, Ikura T, Nagao K, Obuse C, Nozaki N, Takahara S, Takao T, Ohkawa Y, Kimura H, Isaka Y. *Histone H4 lysine 20 acetylation is associated with gene repression in human cells.* Scientific Reports, 2016 Apr 11;6:24318.

38. Kikuchi H, Takami Y, Nakayama T, *GCN5: a supervisor in all-inclusive control of vertebrate cell cycle progression through transcription regulation of various cell cycle-related genes.* Gene, 2005 Feb 28;347(1):83-97.

39. Carrassa L, Damia G, *DNA damage response inhibitors: Mechanisms and potential applications in cancer therapy.* Cancer treatment reviews, 2017 Nov;60:139-151.

40. Lenden Hasse H, Lescale C, Bianchi JJ, Yu W, Bedora-Faure M, Deriano L, *Generation and CRISPR/Cas9 editing of transformed progenitor B cells as a pseudo-physiological system to study DNA repair gene function in V(D)J recombination.* Journal of Immunological Methods, 2017 Dec;451:71-77.

41. Carmona LM, Fugmann SD, Schatz DG, *Collaboration of RAG2 with RAG1-like proteins during the evolution of V(D)J recombination.* Genes and Developmen, 2016 Apr 15;30(8):909-17.

42. Zhao L, Washington MT, *Translesion Synthesis: Insights into the Selection and Switching of DNA Polymerases.* Genes (Basel), 2017 Jan 10;8(1). pii: E24.

43. Budzko L, Jackowiak P, Kamel K, Sarzynska J, Bujnicki JM, Figlerowicz M, *Mutations in human AID differentially affect its ability to deaminate cytidine and 5-methylcytidine in ssDNA substrates in vitro.* Scientific Reports, 2017 Jun 20;7(1):3873.

44. Hultdin M, Grönlund E, Norrback K, Eriksson-Lindström E, Just T, Roos G. *Telomere analysis by fluorescence in situ hybridization and flow cytometry.* Nucleic Acids Res, 1998 Aug 15;26(16):3651-6.

45. Ma Y, Silveri L, LaCava J, Dokudovskaya S, *Tumor suppressor NPRL2 induces ROS production and DNA damage response.* Scientific Reports, 2017 Nov 10;7(1):15311.

46. Rother MB, van Attikum H, *DNA repair goes hip-hop: SMARCA and CHD chromatin remodellers join the break dance.* Phil. Trans. R. Soc. B, 2017 Oct 5;372(1731). pii: 20160285.

47. Bahjat M, Guikema JEJ, *The Complex Interplay between DNA Injury and Repair in Enzymatically Induced Mutagenesis and DNA Damage in B Lymphocytes.* International Journal of Molecular Sciences, 2017 Aug 30;18(9). pii: E1876.

48. Löbrich M, Jeggo P, *A Process of Resection-Dependent Nonhomologous End Joining Involving the Goddess Artemis.* Trends Biochem Sci, 2017 Sep;42(9):690-701.

49. Xing M, Yang M, Huo W, et al, *Interactome analysis identifies a new paralogue of XRCC4 in non-homologous end joining DNA repair pathway.* Nature Community, 2015 Feb 11;6:6233.

50. Church M, Smith KC, Alhussain MM, Pennings S, Fleming AB, *Sas3 and Ada2(Gcn5)-dependent histone H3 acetylation is required for transcription elongation at the de-repressed FLO1 gene.* Nucleic Acids Research, 2017 May 5;45(8):4413-4430.

51. Hammel M, Yu Y, Fang S, Lees-Miller SP, Tainer JA, *XLF regulates filament architecture of the XRCC4·ligase IV complex.* Structure, 2010 Nov 10;18(11):1431-42

52. Rosenberg N, Baltimore D, Scher CD, *In vitro transformation of lymphoid cells by Abelson murine leukemia virus.* PNAS, 1975 May;72(5):1932-6.

53. Nakamura M, Kondo S, Sugai M, Nazarea M, Imamura S, Honjo T, *High frequency class switching of an IgM+ B lymphoma clone CH12F3 to IgA+ cells.* International Immunology, 1996 Feb;8(2):193-201.

54. Nicolas L, Cols M, Choi JE, Chaudhuri J, Vuong B, *Generating and repairing genetically programmed DNA breaks during immunoglobulin class switch recombination.* F1000Res, 2018 Apr 13;7:458.

55. Verkaik NS, Esveldt-van Lange RE, van Heemst D, Brüggenwirth HT, Hoeijmakers JH, Zdzienicka MZ, van Gent DC, *Different types of V(D)J recombination and end-joining defects in DNA double-strand break repair mutant mammalian cells.* European Journal of Immunology, 2002 Mar;32(3):701-9.

56. Hsieh P, Zhang Y, *The Devil is in the details for DNA mismatch repair,* PNAS, 2017 Apr 4;114(14):3552-3554.

57. Jeggo PA, Löbrich M, *DNA non-homologous end-joining enters the resection arena.* Oncotarget, 2017 Oct 26;8(55):93317-93318.

58. Rommel PC, Oliveira TY, Nussenzweig MC, Robbiani DF, *RAG1/2 induces genomic insertions by mobilizing DNA into RAG1/2-independent breaks.* Journal of Experimental Medicine, 2017 Mar 6;214(3):815-831.

59. Bu P, Evrard YA, Lozano G, Dent SY, *Loss of Gcn5 acetyltransferase activity leads to neural tube closure defects and exencephaly in mouse embryos.* Mol Cell Biol, 2007 May;27(9):3405-16.

60. Cai Q, Wang JJ, Fu B, Ying SH, Feng MG, *Gcn5-dependent histone H3 acetylation and gene activity is required for the asexual development and virulence of Beauveria bassiana.* Environmental Microbiology, 2018 Apr;20(4):1484-1497.

61. Carter RJ, Parsons JL, *Base Excision Repair, a Pathway Regulated by Posttranslational Modifications*. Molecular Cell Biology, 2016 May 2;36(10):1426-37.

62. Rada C, Williams GT, Nilsen H, Barnes DE, Lindahl T, Neuberger MS, *Immunoglobulin isotype switching is inhibited and somatic hypermutation perturbed in UNG-deficient mice.* Current Biology, 2002 Oct 15;12(20):1748-55.

63. Arya R, Bassing CH, *V(D)J Recombination Exploits DNA Damage Responses to Promote Immunity.* Trends Genet, 2017 Jul;33(7):479-489.

64. Naviaux RK, Costanzi E, Haas M, Verma IM, *The pCL vector system: rapid production of helper-free, high-titer, recombinant retroviruses.* J Virol, 1996 Aug;70(8):5701-5.

65. Rickert RC, Roes J, Rajewsky K, *B lymphocyte-specific, Cre-mediated mutagenesis in mice.* Nucleic Acids Reseach, 1997 Mar 15;25(6):1317-8.

66. Ranallo RT, Struhl K, Stargell LA, *A TATA-binding protein mutant defective for TFIID complex formation in vivo.* Molecular and Cellular Biology, 1999 Jun;19(6):3951-7.

67. Chitale S, Richly H, *DICER and ZRF1 contribute to chromatin decondensation during nucleotide excision repair.* Nucleic Acids Research, 2017 Jun 2;45(10):5901-5912.

68. Ochi T, Blackford AN, Coates J, Jhujh S, et al, *DNA repair. PAXX, a paralog of XRCC4 and XLF, interacts with Ku to promote DNA double-strand break repair.* Science, 2015 Jan 9;347(6218):185-188.

69. Fazzio TG, *Regulation of chromatin structure and cell fate by R-loops.* Transcription. 2016 Aug 7;7(4):121-6.

70. Kumar V, Alt FW, Frock RL, *PAXX and XLF DNA repair factors are functionally redundant in joining DNA breaks in a G1-arrested progenitor B-cell line.* PNAS, 2016 Sep 20;113(38):10619-24.

71. Kumar V, Alt FW, Oksenych V, *Functional overlaps between XLF and the ATM-dependent DNA double strand break response.* DNA Repair (Amst), 2014 Apr;16:11-22.

72. Wang JL, Duboc C, Wu Q, Ochi T, Liang S, Tsutakawa SE, Lees-Miller SP, Nadal M, Tainer JA, Blundell TL, Strick TR, *Dissection of DNA double-strand-break repair using novel single-molecule forceps.* Nature Structure Molecular Biology, 2018 Jun;25(6):482-487.

73. Lin W, Zhang Z, Srajer G, Chen YC, Huang M, Phan HM, Dent SY, *Proper expression of the Gcn5 histone acetyltransferase is required for neural tube closure in* mouse embryos. Development dynamics, 2008 Apr;237(4):928-40.

74. Hoffman W, Lakkis FG, Chalasani G, *B Cells, Antibodies, and More*. Clin J Am Soc Nephrol, 2016 Jan 7;11(1):137-54

75. Liu X, Shao Z, Jiang W, Lee BJ, Zha S, *PAXX promotes KU accumulation at DNA breaks and is essential for end-joining in XLF-deficient mice.* Nature Communication, 2017 Jan 4;8:13816.

76. Xu W, Edmondson DG, Evrard YA, Wakamiya M, Behringer RR, Roth SY, *Loss of Gcn5l2 leads to increased apoptosis and mesodermal defects during mouse development.* Nature Genetics, 2000 Oct;26(2):229-32.

77. Yamauchi T, Yamauchi J, Kuwata T, Tamura T, Yamashita T, Bae N, Westphal H, Ozato K, Nakatani Y, *Distinct but overlapping roles of histone acetylase PCAF and of the closely related PCAF-B/GCN5 in mouse embryogenesis.* PNAS, 2000 Oct 10;97(21):11303-6.

78. Saito Y, Sugimoto C, Mituyama T, Wakao H, *Epigenetic silencing of V(D)J recombination is a major determinant for selective differentiation of mucosal-associated invariant t cells from induced pluripotent stem cells.* PLoS One, 2017 Mar 27;12(3): e0174699.